

# Boundary states and finite size effects in sine-Gordon model with Neumann boundary condition

Z. Bajnok, L. Palla\* and G. Takács

March 27, 2022

*Institute for Theoretical Physics  
Eötvös University  
H-1117 Budapest, Pázmány P. sétány 1 A-ép, Hungary*

## Abstract

The sine-Gordon model with Neumann boundary condition is investigated. Using the bootstrap principle the spectrum of boundary bound states is established. Somewhat surprisingly it is found that Coleman-Thun diagrams and bound state creation may coexist. A framework to describe finite size effects in boundary integrable theories is developed and used together with the truncated conformal space approach to confirm the bound states and reflection factors derived by bootstrap.

PACS codes: 64.60.Fr, 11.10.Kk

Keywords: sine-Gordon model, boundary conditions, bound states, bootstrap, finite size effects, truncated conformal space approach

arXiv:hep-th/0106069v3 2 Jul 2001

---

\*Corresponding author's e-mail: palla@ludens.elte.hu

# 1 Introduction

In 2 dimensions certain integrable quantum field theories can be restricted to the  $x \leq 0$  half line by imposing suitable boundary conditions without destroying their integrability [1]. In addition to their theoretical interest, these models have important physical applications in various impurity problems (for a review see [2]).

An example is provided by the sine-Gordon model: as was argued in [1], its boundary version:

$$S = \int_{-\infty}^{\infty} dt \int_{-\infty}^0 dx \mathcal{L}_{SG} - \int_{-\infty}^{\infty} dt V_B(\Phi_B), \quad \mathcal{L}_{SG} = \frac{1}{2}(\partial_\mu \Phi)^2 - \frac{m^2}{\beta^2}(1 - \cos(\beta\Phi)), \quad (1.1)$$

(where  $\Phi(x, t)$  is a scalar field,  $\beta$  is a real dimensionless coupling and  $\Phi_B(t) = \Phi(x, t)|_{x=0}$ ) preserves the integrability of the bulk if the boundary potential is chosen as

$$V_B(\Phi_B) = -M_0 \cos\left(\frac{\beta}{2}(\Phi_B - \phi_0)\right),$$

where  $M_0$  and  $\phi_0$  are free parameters. A novel feature of the boundary sine-Gordon model (BSG) is the appearance of a complicated spectrum of boundary bound states (BBS) in addition to the well known bulk ones [1]-[4], [5]. The complete spectrum of these bound states and a full explanation of all the poles are known only for BSG with Dirichlet boundary conditions (which corresponds to taking  $M_0 \rightarrow \infty$ ,  $\Phi_B(t) \equiv \phi_0$ ) [4].

In this paper we investigate the bound state spectrum in sine-Gordon model with Neumann boundary condition (SGN). This boundary condition is in a sense the opposite limit to Dirichlet ( $M_0 = 0$ , thus  $\phi_0$  becoming irrelevant) and has interesting properties as the non conservation of topological charge. Furthermore any BSG model, which is not Dirichlet, behaves in the ultraviolet limit as if it had Neumann boundary condition.

We determine the spectrum of boundary bound states by using the bootstrap principle and give in fact an inductive self consistent proof of their existence. We also give the explanation of all the poles in the various reflection factors in terms of these bound states and Coleman-Thun diagrams [6]. The importance of Coleman-Thun diagrams in the context of boundary bootstrap was first emphasized in [7]. An interesting feature of SGN is that we find instances when Coleman-Thun diagrams and bound state creation coexist (a similar phenomenon was previously observed in the case of boundary Yang-Lee theory [7]). To discover this one has to compute and compare the residues of Coleman-Thun diagrams and the reflection factors, thus one has to go beyond the usual argument that checks only the existence of a diagram with the required pole.

Once we know the spectrum of SGN on the infinite half line the next step is to inquire how it is changing when the model is restricted to a finite line segment  $0 \leq x \leq L$  with suitable boundary conditions. We develop a transfer matrix formalism and use it to discuss the description of boundary bound states in this setting in some detail. Since the resulting finite volume spectra depend on the reflection factors, they provide an ideal laboratory to check these reflection factors, if we can measure the spectra independently.

To this end we develop the truncated conformal space approach (TCSA) [8] to SGN. Determining the finite volume spectra numerically by using TCSA we are able to compare them to the theoretical predictions, and the complete agreement we find gives a strong evidence for the correctness of the various bound states and reflection factors.

The paper is organized as follows: in the next section we describe some classical solutions of SGN and show that the semi-classical quantization of the boundary breathers explains a part of the poles in the breathers reflection factors on non excited boundary. In section 3, using the bootstrap principle, we derive the spectrum of boundary bound states and the associated reflection factors. Section 4 is devoted to the discussion of finite size effects in a large volume  $L$ , with some non trivial boundary conditions at the ends of  $L$ . In section 5, as the main step of TCSA, the Hamiltonian of BSG on  $0 \leq x \leq L$  is described as that of a bulk and boundary perturbed free boson with appropriate boundary conditions. We compare in detail the TCSA data and the theoretical predictions in section 6. We make our conclusions in section 7. The paper is closed by three appendices: in Appendix A we give in details the proof of the existence of the boundary bound states. In Appendix B we explain the poles of the soliton and breather reflection factors. Finally, in Appendix C we review those aspects of boundary  $c = 1$  theories that are necessary to set up our TCSA.

## 2 A few classical solutions and the semiclassical spectrum of boundary breathers in SGN

In boundary sine-Gordon theory with Neumann boundary condition (SGN) the boundary potential is absent:  $M_0 = 0$ . As a result,  $\Phi(x, t)$  satisfies free boundary condition at  $x = 0$ :  $\partial_x \Phi(x, t)|_{x=0} = 0$ . This boundary condition preserves the  $\Phi \leftrightarrow -\Phi$  charge conjugation symmetry ( $\mathbf{C}$  symmetry) of the bulk theory, but violates the conservation of topological charge. This can be seen already on the simplest classical solution of SGN, describing the scattering of a classical soliton on the boundary. This solution,  $\tilde{\Phi}_s(x, t)$ , is obtained by restricting to the  $x \leq 0$  half line the  $\Phi_{SA}(x, t)$  soliton anti soliton solution of the bulk theory:

$$\tilde{\Phi}_s(x, t) \equiv \Phi_{SA}(x, t) = \frac{4}{\beta} \arctan \left[ \frac{\sinh(umt/\sqrt{1-u^2})}{u \cosh(mx/\sqrt{1-u^2})} \right], \quad \text{for } -\infty < x \leq 0. \quad (2.1)$$

(Since  $\partial_x \Phi_{SA}(x, t)|_{x=0} = 0$  it indeed satisfies the Neumann boundary condition). This solution exhibits that the incident soliton reflects as an anti soliton from the Neumann boundary, i.e. topological charge changes by two units in this scattering.

Another observation that plays an important role in the sequel is that the ‘standing’ breather solution of the bulk SG, oscillating with period  $\tau$  around  $x = 0$ :

$$\Phi_\tau(x, t) = \frac{4}{\beta} \arctan \left[ \sqrt{(\tilde{\tau})^2 - 1} \frac{\sin(mt/\tilde{\tau})}{\cosh(mx\sqrt{1-(\tilde{\tau})^{-2}})} \right], \quad \tilde{\tau} = \frac{m\tau}{2\pi}, \quad (2.2)$$

also satisfies  $\partial_x \Phi_\tau(x, t)|_{x=0} = 0$ . Therefore the classical breather solution, bound to the wall at  $x = 0$  is given by

$$\tilde{\Phi}_\tau(x, t) = \Phi_\tau(x, t), \quad \text{for } -\infty < x \leq 0. \quad (2.3)$$

In SGN ‘boundary dependent’ simple poles are found in the reflection factors of the various breathers [3] that may describe boundary bound states (BBS). In the reflection factor of the  $n$ -th breather,  $B^n$ , this pole is located at the  $\theta = inp\pi/2$ <sup>1</sup> value of the purely imaginary

---

<sup>1</sup>The parameter  $p$  is determined by the sine-Gordon coupling constant as  $p = \beta^2/(8\pi - \beta^2)$ .

rapidity, so that if it really corresponds to a BBS, then the energy of this state above the ground state is

$$e_n - e_0 = M \sin(np\pi). \quad (2.4)$$

In the form of two lemmas sufficient conditions were given in [4] that guarantee that a simple pole in a reflection factor cannot be explained by the Coleman-Thun mechanism [6], i.e. that it describes a bound state. However, these conditions are not satisfied for any of the poles above, thus the question whether they correspond to BBS remains open. Furthermore, a Coleman-Thun explanation of a subset of the poles is given by the solitonic version of diagram (c) on Fig.(3.2), when the index  $n$  of the breather satisfies  $n > 1/(2p)$ . (This is discussed in detail in the next section). We clarify the status of the poles for  $n < 1/(2p)$  below by showing that the energies associated to them as hypothetical BBS match exactly with the spectrum of bound states obtained by semi-classical quantization from the classical boundary breather solutions of SGN (2.2-2.3). We achieve this by adapting to this problem the semi-classical derivation of the breather spectrum in the bulk sine-Gordon theory as given in the classic paper [9].

The semi-classical (WKB) quantization of any periodic classical solution,  $\phi_{cl}$  in a field theory can be summarized by the equations:

$$-\frac{\partial}{\partial \tau} \left[ S_{cl}(\phi_{cl}) + S_{ct}(\phi_{cl}) - \sum_{i=0}^{\infty} (n_i + \frac{1}{2}) h\nu_i(\phi_{cl}) \right] = E, \quad (2.5)$$

$$W_{\{n_i\}}(E) = 2K\pi\hbar, \quad K \text{ integer}, \quad (2.6)$$

where

$$W_{\{n_i\}}(E) = S_{cl}(\phi_{cl}) + S_{ct}(\phi_{cl}) + E\tau(\phi_{cl}) - \sum_{i=0}^{\infty} (n_i + \frac{1}{2}) h\nu_i(\phi_{cl}). \quad (2.7)$$

Here  $\tau(\phi_{cl})$  denotes the period of the classical solution,  $\nu_i(\phi_{cl})$  stand for its stability frequencies (that characterize the quasi periodicity  $\xi_i(x, t+\tau) = e^{i\nu_i} \xi_i(x, t)$  of the solutions of  $\left[ -\frac{\partial^2}{\partial t^2} + \frac{\partial^2}{\partial x^2} - \left( \frac{\partial^2 U}{\partial \phi^2} \right)_{\phi_{cl}} \right] \xi_i(x, t) = 0$ ), and  $n_i$  are a set of non negative integers. Furthermore the subscript ‘ct’ stands for counter term contributions, whose effect is to cancel divergences in the infinite sums. Eq.(2.5) picks out the appropriate classical periodic solution for a given  $E$  and a given set of integers  $n_i$ . Then those values of  $E$  which satisfy Eq.(2.6-2.7), give the renormalized bound state energies.

With the Neumann boundary condition the boundary potential is absent, and as  $\mathcal{L}_{SG}(\Phi_\tau)$  is symmetric for  $x \mapsto -x$ , we easily obtain

$$S_{cl}(\tilde{\Phi}_\tau) = \frac{16\pi}{\beta^2} \left( \arccos \left( \frac{1}{\tilde{\tau}} \right) - \sqrt{(\tilde{\tau})^2 - 1} \right), \quad (2.8)$$

which is just *half* of the corresponding expression in the bulk theory. The stability frequencies for  $\tilde{\Phi}_\tau$  are the *same* as for  $\Phi_\tau$ , but the  $\tilde{\xi}(x, t)$  fluctuations must also satisfy  $\partial_x \tilde{\xi}(x, t)|_{x=0} = 0$ . Therefore only half of the bulk stability fluctuations appear in the Neumann problem, namely those that are even under  $x \mapsto -x$ , (and the same applies to the fluctuations contributing to the vacuum energy  $E_{vac}$  appearing in the counter term). Thus effectively we must take  $\sum \tilde{\nu}_i = \frac{1}{2} \sum \nu_i$ . To obtain the basic boundary bound states we set all  $n_i = 0$ , and using the explicit form of the counter-terms and the sums over  $\nu_i$  as given in [9] we find finally

$$S_{ct}(\tilde{\Phi}_\tau) - \sum \frac{1}{2} \tilde{\nu}_i = -\frac{\beta^2}{8\pi} S_{cl}(\tilde{\Phi}_\tau). \quad (2.9)$$

Using these results in Eq.(2.5, 2.7) leads to

$$\tilde{E} = \frac{m}{\pi p} \frac{\sqrt{(\tilde{\tau})^2 - 1}}{\tilde{\tau}}, \quad W(\tilde{E}) = \frac{2}{p} \arcsin\left(\frac{\tilde{E} p \pi}{m}\right). \quad (2.10)$$

As a result the quantization condition,  $W(\tilde{E}_K) = 2\pi K$ , gives

$$\tilde{E}_K = M \sin(Kp\pi), \quad (2.11)$$

where  $M = \frac{m}{p\pi}$  is the semi-classical soliton mass. Clearly this reproduces (2.4). Since  $\tau(\tilde{E}_K) \sim \frac{1}{\cos(Kp\pi)}$  the range of  $K$ -s where bound states exist (i.e where  $\tau(\tilde{E}_K) < \infty$ ) is  $K < 1/(2p)$ .

### 3 Boundary bound state spectrum from bootstrap principle

In this Section we determine the spectrum of boundary excitations, the related soliton and breather reflection factors and show how their poles can be explained in terms of on-shell diagrams. We start with a summary of the bulk scattering properties and then review the result of Ghoshal and Zamolodchikov concerning the reflection factors of the soliton and breathers on the non-excited boundary. From their pole structure and the bootstrap equation we conjecture the minimal spectrum of the excited boundary states (or with other words boundary bound states), and prove in Appendix A that they can be created by successive soliton absorptions on the wall at purely imaginary rapidity. Having determined the reflection factors we explain all their poles in terms of on-shell diagrams which correspond either to some Coleman-Thun mechanism or creation of boundary bound states. In this study we rely heavily on the machinery worked out in [4] for the Dirichlet case. However, in contrast to the Dirichlet case we find instances when a Coleman-Thun type diagram happens to give a pole of the same order as the reflection amplitude has, but with wrong residue, thus leaving the possibility of excited boundary state creation at the same time.

#### 3.1 Bulk scattering properties

In the bulk SG model any scattering amplitude among solitons and anti solitons factorizes into a product of two particle scattering amplitudes, of which the independent ones are [10]

$$\begin{aligned} a(u) = S_{++}^{++}(u) = S_{--}^{--}(u) &= - \prod_{l=1}^{\infty} \left[ \frac{\Gamma(2(l-1)\lambda - \frac{\lambda u}{\pi}) \Gamma(2l\lambda + 1 - \frac{\lambda u}{\pi})}{\Gamma((2l-1)\lambda - \frac{\lambda u}{\pi}) \Gamma((2l-1)\lambda + 1 - \frac{\lambda u}{\pi})} / (u \rightarrow -u) \right] \\ b(u) = S_{+-}^{+-}(u) = S_{-+}^{-+}(u) &= \frac{\sin(\lambda u)}{\sin(\lambda(\pi - u))} a(u) \quad ; \quad \lambda = \frac{8\pi}{\beta^2} - 1 = \frac{1}{p}, \\ c(u) = S_{+-}^{-+}(u) = S_{-+}^{+-}(u) &= \frac{\sin(\lambda\pi)}{\sin(\lambda(\pi - u))} a(u) \quad ; \quad u = -i\theta. \end{aligned}$$

Since we are concentrating on the bound state poles located at purely imaginary rapidities we use the variable  $u$  instead of  $\theta$  and refer to it as the rapidity from now on in this Section. The other scattering amplitudes can be described in terms of the functions

$$\{y\} = \frac{\left(\frac{y+1}{2\lambda}\right) \left(\frac{y-1}{2\lambda}\right)}{\left(\frac{y+1}{2\lambda} - 1\right) \left(\frac{y-1}{2\lambda} + 1\right)}, \quad (x) = \frac{\sin\left(\frac{u}{2} + \frac{x\pi}{2}\right)}{\sin\left(\frac{u}{2} - \frac{x\pi}{2}\right)},$$

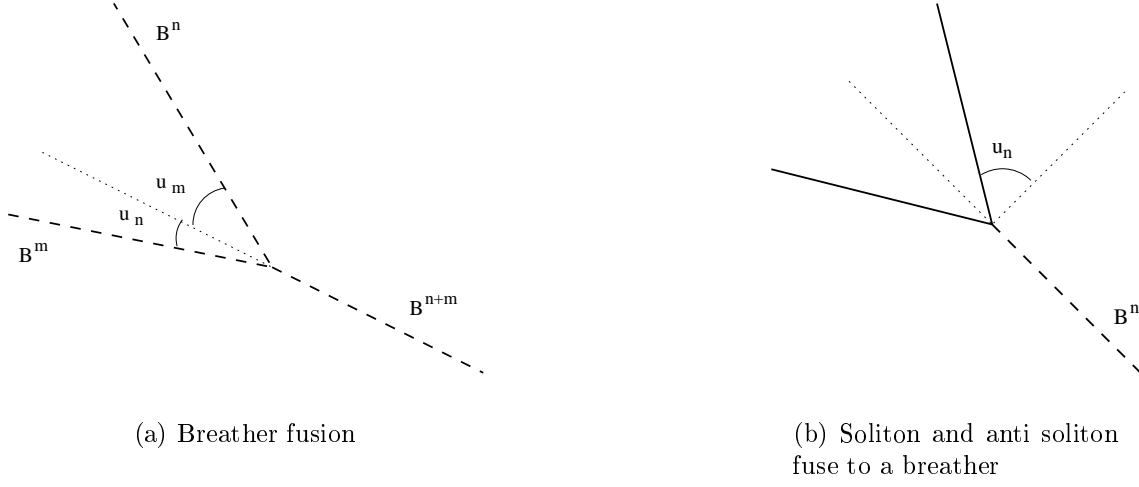


Figure 3.1: Bulk vertices

as follows. For the scattering of the breathers  $B^n$  and  $B^m$  with  $n \geq m$  and relative rapidity  $u$  we have [10]

$$S^{nm}(u) = S_{nm}^{nm}(u) = \{n+m-1\}\{n+m-3\} \dots \{n-m+3\}\{n-m+1\} ,$$

while for the scattering of the soliton (anti soliton) and  $B^n$  we have

$$S^n(u) = S_{+n}^{+n}(u) = S_{-n}^{-n}(u) = \{n-1+\lambda\}\{n-3+\lambda\} \dots \begin{cases} \{1+\lambda\} & \text{if } n \text{ is even} \\ -\sqrt{\{\lambda\}} & \text{if } n \text{ is odd} \end{cases} .$$

All the poles of the scattering amplitudes in the physical strip originate from virtual processes either in the forward or in the cross channel of the diagrams (a-b) on Fig.(3.1), where the useful definition

$$u_n = \frac{n\pi}{2\lambda}$$

was also introduced.<sup>2</sup> For each such process a coupling as  $f_{nm}^{n+m}$  or  $f_{+-}^n$  can be attributed and it is known that  $f_{+-}^n = (-1)^n f_{-+}^n$ .

### 3.2 Reflection factors on ground state boundary

The reflection factor of the soliton on the ground state Neumann boundary was found by Ghoshal and Zamolodchikov [1]. For the topological charge preserving process, (i.e. when a soliton (anti soliton) reflects as soliton (anti soliton)), we have

$$P(u) = \cos(\lambda u) R_0(u) \sigma\left(\frac{\pi}{2}(\lambda+1), u\right) \sigma(0, u) ,$$

where

$$R_0(u) = \prod_{l=1}^{\infty} \left[ \frac{\Gamma(4l\lambda - \frac{2\lambda u}{\pi}) \Gamma(4\lambda(l-1) + 1 - \frac{2\lambda u}{\pi})}{\Gamma((4l-3)\lambda - \frac{2\lambda u}{\pi}) \Gamma((4l-1)\lambda + 1 - \frac{2\lambda u}{\pi})} / (u \rightarrow -u) \right]$$

---

<sup>2</sup>On all the space-time diagrams time develops from top to bottom. Solitons (or anti solitons) are denoted by solid lines, while breathers by dashed ones.

is the boundary condition independent part and

$$\sigma(x, u) = \frac{\cos x}{\cos(x + \lambda u)} \prod_{l=1}^{\infty} \left[ \frac{\Gamma(\frac{1}{2} + \frac{x}{\pi} + (2l-1)\lambda - \frac{\lambda u}{\pi}) \Gamma(\frac{1}{2} - \frac{x}{\pi} + (2l-1)\lambda - \frac{\lambda u}{\pi})}{\Gamma(\frac{1}{2} - \frac{x}{\pi} + (2l-2)\lambda - \frac{\lambda u}{\pi}) \Gamma(\frac{1}{2} + \frac{x}{\pi} + 2l\lambda - \frac{\lambda u}{\pi})} / (u \rightarrow -u) \right]$$

describes the boundary condition dependence.<sup>3</sup>The poles of  $\sigma(x, u)$  in the physical strip are located at  $u = \frac{x}{\lambda} - u_{2k+1}$  or at  $\pi - \frac{x}{\lambda} + u_{2k+1}$ ,  $k \geq 0$ ; and it has no zero there.

For the topological charge changing process, (when the soliton (anti soliton) comes back as anti soliton (soliton)), we have

$$Q(u) = \frac{\sin(\lambda u)}{\sin(\frac{\lambda \pi}{2})} P(u) .$$

Note that the topological charge is changed by two in this process, thus the parity of the soliton number is conserved and we have an odd and an even sector.

The breather reflection factors share the same structure as the solitonic ones as a consequence of the general expression in [3]. For Neumann boundary condition and breather  $B^n$  they have the following form

$$R^{(n)}(u) = R_0^{(n)}(u) S^{(n)}\left(\frac{\pi}{2}(\lambda + 1), u\right) S^{(n)}(0, u)$$

where

$$R_0^{(n)}(u) = \frac{(\frac{1}{2}) (\frac{n}{2\lambda} + 1)}{(\frac{n}{2\lambda} + \frac{3}{2})} \prod_{l=1}^{n-1} \frac{(\frac{l}{2\lambda}) (\frac{l}{2\lambda} + 1)}{(\frac{l}{2\lambda} + \frac{3}{2})^2} ; \quad S^{(n)}(x, u) = \prod_{l=\frac{1-n}{2}}^{\frac{n-1}{2}} \frac{(\frac{x}{\lambda\pi} - \frac{1}{2} + \frac{l}{\lambda})}{(\frac{x}{\lambda\pi} + \frac{1}{2} + \frac{l}{\lambda})}$$

In general  $R_0^{(n)}$  would describe the boundary independent properties and the other factors would give the boundary dependent ones. In the Neumann case, however, there are coincidences among the poles and zeros of the various factors and it is better to rewrite the reflection factor as

$$R^{(n)}(u) = \langle 2n-1 \rangle \langle 2n-3+4\lambda \rangle \dots \langle 2(n-k)-1+(1-(-1)^k)2\lambda \rangle \dots \begin{cases} \langle 1 \rangle & \text{if } n \text{ is odd} \\ \langle 1+4\lambda \rangle & \text{if } n \text{ is even} \end{cases} ,$$

where

$$\langle y \rangle = \frac{(\frac{y+1}{4\lambda}) (\frac{y-1}{4\lambda})}{(\frac{y+1}{4\lambda} - \frac{1}{2}) (\frac{y-1}{4\lambda} + \frac{1}{2})}$$

is the ‘‘half-block’’ with respect to  $\{y\}$ .

### 3.2.1 Pole analysis

Now consider the poles of the soliton reflection factor  $P(u)$ .

- There are boundary independent poles in the physical strip due to the factor  $R_0(u)$ . They are located at  $u_n$ ,  $n = 1, 2, \dots$  from which every odd is canceled by the zero of  $\cos(\lambda u)$ . The remaining poles can be described by diagram (a) on Fig.(3.2). This is consistent with the fact that the  $\mathbf{C}$  symmetric Neumann boundary can emit and absorb only even breathers with zero momentum.

---

<sup>3</sup>The function  $\sigma(x, u)$  has among others the property  $\sigma(x, u)\sigma(x, -u) = \frac{\cos^2 x}{\cos(x+\lambda u)\cos(x-\lambda u)}$  which corrects a typo in [1] and [3].

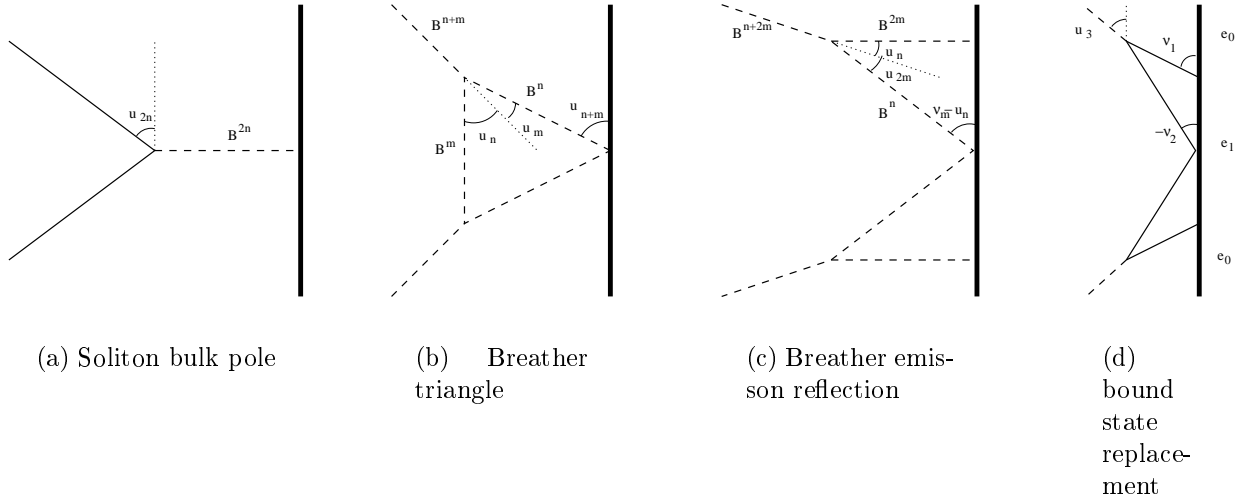


Figure 3.2: A few boundary diagrams

- The boundary dependent poles in the physical strip are located at

$$\nu_n = \frac{\pi}{2} - u_{2n} \quad ; \quad n = 0, 1, \dots, \left\lfloor \frac{\lambda}{2} \right\rfloor$$

The pole at  $\frac{\pi}{2}$  is responsible for the emission and absorption of a zero momentum soliton or anti soliton. For each of the other poles we associate a boundary bound state with energy

$$e_n - e_0 = M \sin u_{2n}$$

From now on we put the boundary ground state energy to zero  $e_0 = 0$  for simplicity.

Clearly the basically bulk process (a) on Fig.(3.2) does not exist for the reflection amplitude  $Q(u)$  and the factor  $\sin(\lambda u)$  takes care of this. The boundary dependent poles of  $Q(u)$  coincide with and can be explained in the same way as those of  $P(u)$ .

Now let us focus on the poles of the breather reflection factors. As a warm-up example consider the reflection factor of the third breather:

$$R^{(3)}(u) = \langle 5 \rangle \langle 3 + 4\lambda \rangle \langle 1 \rangle$$

- It has a simple bulk pole at  $\frac{\pi}{2} - u_3$  whose explanation depends on the value of the parameter  $\lambda$ . If  $B^6$  is in the spectrum then we can use the ‘all-breather’ version of diagram (a). On this we mean by replacing each soliton line by a  $B^3$  line having rapidity  $\frac{\pi}{2} - u_3$  and  $B^6$  is formed at the vertex. Now if  $B^6$  is not in the spectrum then the soliton version of diagram (b) applies. In this case the breather triangle is turned into a soliton-anti soliton triangle.
- The pole at  $\frac{\pi}{2} - u_1$  is of second order and can be explained by diagram (c).
- The pole at  $u_3$  can be explained by the soliton version of diagram (c) for  $3 > \left\lfloor \frac{\lambda}{2} \right\rfloor$  (which is necessary to guarantee that the soliton in the middle also travels towards the wall). This diagram gives a second order pole and the reflection factor has no zero at  $-\nu_3 = u_6 - \frac{\pi}{2}$ . We have an analogous diagram, however, by changing the amplitude



$P(u)$  for  $Q(u)$ . They differ by a factor of  $\sin(-\lambda\nu_3)/\sin(\frac{\lambda\pi}{2}) = -(-1)^3$  but we know that  $f_{+-}^3 = (-1)^3 f_{-+}^3$ . This gives the sign difference which is responsible for the Coleman-Thun type cancellation in the sum of the two diagrams. In the  $3 \leq [\frac{\lambda}{2}]$  case we have a boundary bound state with energy

$$e_3 = M_3 \cos u_3 = 2M \sin u_3 \cos u_3 = M \sin u_6 ,$$

which is exactly the same as the boundary bound state created by the soliton. The identity of these two boundary bound states can also be confirmed by showing the agreement of the other higher spin conserved charges.

- For the other two poles at  $u_1$  and  $u_2$  we have diagram (b). In the case of  $u_2$  the second breather hits the boundary while in the case of  $u_1$  the first.

We could be satisfied now and turn to the general case. There is a subtlety, however, since we have not computed the residues. Performing the computation reveals that the residues of the reflection factors and diagrams agree except for the pole  $u_1$  where they have different signs. Thus we must assume that a boundary bound state exists with energy  $M_3 \cos u_1 = e_1 + e_2$ . We note that in the Neumann case the bulk pole of  $R_0^{(3)}(u)$  and a boundary pole of  $S^{(3)}(\frac{\pi}{2}(\lambda+1), u)$  at  $u_1$  coincide but a zero in the boundary factor reduces the singularity to first order. If we move a bit away from the Neumann point, when the boundary dependent part becomes  $S^{(3)}(\frac{\pi}{2}(\lambda+1) - \delta\lambda, u)$ , the two poles split and the bulk pole at  $u_1$  can be described by the diagram above, while the pole at  $u_1 - \delta$  corresponds to a boundary bound state. Computing the residue and taking the  $\delta \rightarrow 0$  limit do not commute, however, resulting in a sign difference. This sign difference persists when the state with energy  $e_2$  is not in the spectrum i.e. for  $u_4 > \frac{\pi}{2}$ . In this case we have diagram (d), where  $B^3$  is decaying into a soliton and an anti soliton. Then the soliton creates the state with energy  $e_1$  on which the other anti soliton is reflecting with rapidity  $u_4 - \frac{\pi}{2}$ . This diagram is naively second order, however, the same Coleman-Thun mechanism that we used in the previous example, takes care of the cancellation.

From this example we can draw two conclusions. First, breathers and solitons can create the same states. Second, even if a diagram describes a pole of the same order as the reflection factor has, the residues do not always coincide, thus allowing the creation of a boundary bound state in the same time.

Now we are ready to discuss the general case. The reflection factor  $R^{(n)}(u)$  has the following poles in the physical strip.

- There is a simple pole at  $\frac{\pi}{2} - u_n$ . It can be explained in terms of the breather version of diagram (a) by forming  $B^{2n}$  or if it is not in the spectrum then by the soliton version of diagram (b).
- The double poles at  $\frac{\pi}{2} - u_{n-2k}$  can be explained by diagram (c).
- For even breathers there is an extra simple pole at  $\frac{\pi}{2}$ . It corresponds to the emission of a zero momentum even breather.
- The simple pole at  $u_n$  corresponds to the creation of the boundary bound state with energy  $e_n = M \sin u_{2n}$ , if it is in the spectrum. Alternatively, it can be explained in terms of the solitonic version of diagram (c) where, just as in the example, a Coleman-Thun type mechanism ensures the pole to be simple.

- If  $n+k$  is even then the pole  $u_k$  is responsible for the creation of a boundary bound state with energy  $e_{\frac{n+k}{2}} + e_{\frac{n-k}{2}}$ , if  $e_{\frac{n+k}{2}}$  is in the spectrum. Alternatively, we have diagram (d) where the state with energy  $e_k$  is created in the middle and the Coleman-Thun argument has to be used for the scattering.
- If, however,  $n+k$  is odd then the pole at  $u_k$  has its explanation in terms of diagram (b).

### 3.3 Excited state reflection factors

We have seen that both the pole of the soliton reflection factor at  $\nu_n$  and the pole of the reflection factor of  $B^n$  at  $u_n$  give rise to a state with energy  $e_n$ . The identity of these two states can be further confirmed by showing that any reflection factors on them agree. Computing these reflection factors from the solitonic and breather bootstrap equations gives identical results. Therefore we denote these common states by  $|n\rangle$ .

In computing the soliton excited state reflection factor we use the

$$P_{|n\rangle}(u) = P(u)S^n(u + u_n)S^n(u - u_n)$$

”soliton-breather” bootstrap equation. The result is

$$P_{|n\rangle}(u) = a_n(u)P(u) \quad ; \quad a_n(u) = \{2n - 1 + \lambda\}\{2n - 3 + \lambda\} \dots \{1 + \lambda\} .$$

We have checked that the purely solitonic bootstrap equation gives the same result. Since the solitonic reflection factor has one extra pole at  $\nu_0 = \frac{\pi}{2}$  we can bootstrap on this pole and obtain  $P_{|0\rangle}(u) = P(u)$ . This means that the ground state is non degenerate, so the creation or annihilation of a soliton or anti soliton does not change the boundary ground state. (We have already used this property in the explanation of the ground state breather poles). The existence of a unique ground state implies that  $\mathbf{C}$  symmetry is not broken. Note, however, that this is strikingly different from the case for Dirichlet boundary condition at  $\xi = \frac{\pi}{2}(\lambda + 1)$ , where one has two vacua and the  $Z_2$  symmetry is spontaneously broken [11].

Repeating the same bootstrap program for the amplitude  $Q(u)$  we arrive at

$$Q_{|n\rangle}(u) = a_n(u)Q(u) .$$

For the breather reflection factors on the excited state  $|n\rangle$  the bootstrap equation takes the form

$$R_{|n\rangle}^{(m)}(u) = R^{(m)}(u)S^{nm}(u + u_n)S^{nm}(u - u_n) .$$

From here we have explicitly

$$R_{|n\rangle}^{(m)}(u) = b_n^m(u)R^{(m)}(u)$$

where

$$b_n^m(u) = \{m + 2n - 1\}\{m + 2n - 3\} \dots \dots \{m + 2n - 1 - 2l\} \dots \begin{cases} \{m - 2n + 1\} & \text{if } m - 2n + 1 > 0 \\ \{2n - m + 1\} & \text{if } 2n - m + 1 > 0 \end{cases} .$$

Let us focus on the solitonic reflection factors  $P_{|n\rangle}(u)$ . The prefactor  $a_n(u)$  has simple poles at  $\nu_0$  and  $\nu_n$  and double poles at  $\nu_k$ ,  $k = 1, 2, \dots, n - 1$ . The locations of these poles are the same as that of  $P(u)$ , thus only the order has increased for  $k \leq n$ . We conjecture, and in fact prove in Appendix A, that the other simple poles at  $\nu_k$ ,  $k > n$ , which do not come from  $a_n(u)$ , are responsible for the creation of the excited boundary bound states with energy  $e_n + e_k$  which we denote by  $|n, k\rangle$ .

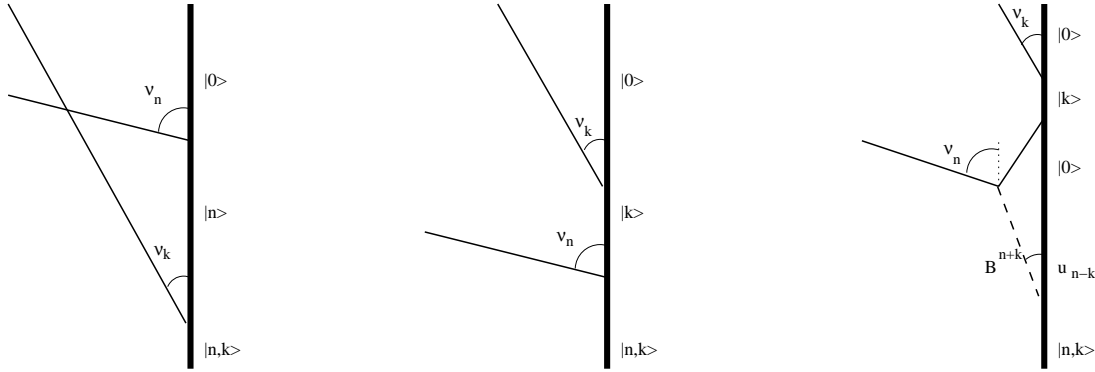


Figure 3.3: Various ways of creating the state  $|n, k\rangle$ .

Now it is interesting to use the integrability of the model. Using the factorizability argument we can shift the soliton trajectory and obtain the three diagrams on Fig.(3.3).

In the first picture the soliton creates the boundary bound states  $|n\rangle$  at an angle  $\nu_n$  then another soliton creates  $|n, k\rangle$  at an angle  $\nu_k$  where  $k > n$ . They scatter on each other at an angle  $u_{2(k-n)}$  which is not proper for forming a breather. Now if we move the second soliton trajectory up we obtain the picture in the middle. Here the soliton at  $\nu_k$  creates the state  $|k\rangle$  then the other soliton reflects on it at an angle  $\nu_n$ . This reflection factor has a third order pole for which diagram (a) on Fig.(B.3) shown in Appendix B can be associated showing the creation of the state  $|n, k\rangle$  as it was expected from consistency. In the third picture the excited boundary  $|k\rangle$  decays by emitting a soliton. This soliton then scatters on the other soliton forming  $B^{n+k}$  with rapidity  $u_{k-n}$  which finally creates the state  $|n, k\rangle$ .

Now we can use any of the processes above (or their breather versions) to compute the reflection amplitudes. They turn out to be

$$P_{|n,k\rangle}(u) = a_n(u)a_k(u)P(u) \quad ; \quad Q_{|n,k\rangle}(u) = a_n(u)a_k(u)Q(u)$$

and

$$R_{|n,k\rangle}^{(m)}(u) = b_n^m(u)b_k^m(u)R^{(m)}(u)$$

From this it is clear how it goes on, so we turn to the description of the spectrum of the boundary bound states and their reflection factors in general.

### 3.4 The spectrum of the boundary bound states and the associated reflection factors

From the previous discussion it is clear that a boundary bound state can be labelled by a sequence of increasing positive integers and denoted by  $|n_1, n_2, \dots, n_k\rangle$  where  $n_i > n_{i-1}$  and  $n_k < \lfloor \frac{\lambda}{2} \rfloor$ . Its energy can be written as

$$m_{|n_1, n_2, \dots, n_k\rangle} = \sum_{j=1}^k M \sin u_{2n_j} = \sum_{j=1}^k e_{n_j}.$$

The first task is to prove the existence of these states. Unfortunately the proof of [4], which uses the breathers to create the boundary bound states, does not apply. This proof is based

on a special property of the breather reflection factors with Dirichlet b.c.-s, namely that to every pole either a bound state or a Coleman-Thun diagram can be associated. In contrast to the Dirichlet case we have shown that Coleman-Thun diagrams and boundary bound state creations may coexist in the Neumann problem. We prove, however, in Appendix A that solitons at reflection angle  $\nu_m$  on the state  $|n_1, n_2, \dots, n_k\rangle$  can create the state  $|n_1, n_2, \dots, n_k, m\rangle$  if  $m > n_k$ . Now the next step is to compute the reflection factors and explain all the poles in terms of diagrams. The computation is quite straightforward and the result is

$$\begin{aligned} P_{|n_1, n_2, \dots, n_k\rangle}(u) &= a_{n_1}(u)a_{n_2}(u) \dots a_{n_k}(u)P(u) \\ Q_{|n_1, n_2, \dots, n_k\rangle}(u) &= a_{n_1}(u)a_{n_2}(u) \dots a_{n_k}(u)Q(u) \end{aligned}$$

and

$$R_{|n_1, n_2, \dots, n_k\rangle}^{(m)}(u) = b_{n_1}^m(u)b_{n_2}^m(u) \dots b_{n_k}^m(u)R^{(m)}(u).$$

Using the factorizability argument leads to the following creation-annihilation rules: For the soliton with rapidity  $\nu_m$

$$|n_1, \dots, n_i, n_{i+1}, \dots, n_k\rangle \longrightarrow |n_1, \dots, n_i, m, n_{i+1}, \dots, n_k\rangle$$

if  $n_i < m < n_{i+1}$ . For  $B^m$  with rapidity  $u_{2n_i+m}$  we have

$$|n_1, \dots, n_i, \dots, n_k\rangle \longrightarrow |n_1, \dots, n_i + m, \dots, n_k\rangle ,$$

while for  $B^{m+l}$  with rapidity  $u_{l-m}$  and  $l > m$  the process is

$$|n_1, \dots, n_i, n_{i+1}, \dots, n_j, n_{j+1}, \dots, n_k\rangle \longrightarrow |n_1, \dots, n_i, m, n_{i+1}, \dots, n_j, l, n_{j+1}, \dots, n_k\rangle .$$

Now the most difficult problem is to explain all the poles of the reflection factors in terms of diagrams. Since it is quite cumbersome we put it in Appendix B.

## 4 Finite size effects in large volume

### 4.1 Bethe-Yang equations for particles in finite volume with boundaries

Imagine putting  $N$  particles in finite volume  $L$ , such that the  $i$ th particle  $A_i$  has mass  $M_i$  and rapidity  $\theta_i$  (which we choose nonnegative since only the absolute value matters, due to reflection on the boundaries), plus some additional internal quantum numbers  $\alpha_i$  (distinguishing it within a multiplet of the same mass  $M_i$ ). Let us denote the reflection factor of the  $i$ th particle on the left/right end of the interval by  $R_L^{(i)}(\theta_i)$  and  $R_R^{(i)}(\theta_i)$ , respectively and the scattering matrix of particles  $A_i$  and  $A_j$  by  $S^{(i,j)}(\theta_i - \theta_j)$ . Obviously in the general case these are matrices with the following structure

$$\begin{aligned} R_L^{(i)}(\theta_i) &= \left\{ R_L^{(i)}(\theta_i)_{\alpha_i}^{\alpha'_i} \right\} , \\ R_R^{(i)}(\theta_i) &= \left\{ R_R^{(i)}(\theta_i)_{\alpha_i}^{\alpha'_i} \right\} , \\ S^{(i,j)}(\theta_i - \theta_j) &= \left\{ S^{(i,j)}(\theta_i - \theta_j)_{\alpha_i \alpha_j}^{\alpha'_i \alpha'_j} \right\} . \end{aligned}$$

We define a family of transfer matrices that acts in  $V_1 \otimes \dots \otimes V_N$ , where  $V_i$  is the internal space labelled by the multiplicity index  $\alpha_i$  of the  $i$ th particle. The transfer matrix  $T_k$  describes a unitary transformation on the wave function resulting from the scattering of  $A_k$  on the other particles and the two boundaries when we take the particle around the volume (starting e.g to the left, reflecting on the left boundary, coming back to the right, reflecting on the right boundary and returning to the original position):

$$T_k^{(1, \dots, N)}(\theta_1, \dots, \theta_N) = R_R^{(k)}(\theta_k) \prod_{j:j \neq k} S^{(j,k)}(\theta_k + \theta_j) R_L^{(k)}(\theta_k) \prod_{j:j \neq k} S^{(j,k)}(\theta_k - \theta_j) .$$

We omitted the multiplicity indices of the matrices (these are indicated by the upper indices in brackets and can be restored easily). The scatterings were performed in a particular order, due to the equations of factorized bulk and boundary scatterings, the order is eventually immaterial: performing the scatterings in any other way results in the same transfer matrix. Another consequence of factorized scattering is that the matrices  $T_k$  form a commuting family for a given set of rapidities. The wave function can be characterized by a vector  $\psi_{\alpha_1 \dots \alpha_N}$  living in the tensor product space, and transforming under all such monodromy operations as:

$$\exp(2iM_k L \sinh(\theta_k)) T_k^{(1, \dots, N)}(\theta_1, \dots, \theta_N) \psi = \psi \quad , \quad k = 1, \dots, N . \quad (4.1)$$

The prefactor in this equation is the phase acquired by  $A_k$  due to its momentum (whose absolute value is  $M_k \sinh \theta_k$ ). Equations (4.1) are the so-called Bethe-Yang equations in the presence of a boundary.

Since the transfer matrices commute, they can be diagonalized simultaneously. Let us denote the eigenvalues of the transfer matrix  $T_k^{(1, \dots, N)}(\theta_1, \dots, \theta_N)$  by  $\lambda_k^{(s)}(\theta_1, \dots, \theta_N)$ , where  $s = 1, \dots, D_N$  enumerates the eigenvalues (with multiplicities) and  $D_N = \dim V_1 \otimes \dots \otimes V_N$ . The corresponding common eigenvectors will be called  $\psi^{(s)}(\theta_1, \dots, \theta_N)$ .

The solutions to the Bethe-Yang equations (4.1) are given by the wave function amplitudes

$$\psi = \psi^{(s)}(\theta_1, \dots, \theta_N)$$

provided that the rapidities solve the equations<sup>4</sup>

$$\exp(2iM_k L \sinh(\theta_k)) \lambda_k^{(s)}(\theta_1, \dots, \theta_N) = 1 \quad , \quad k = 1, \dots, N \quad (4.2)$$

for some (fixed)  $s$ . These equations effectively describe the quantization of momentum in finite volume with boundaries. The total kinetic energy of the particles is then given by

$$E_{\text{kin}} = \sum_{j=1}^N M_j \cosh \theta_j ,$$

which is the energy difference with respect to the state with no particles in this approximation.

The above calculation supposes that the particles do not overlap with each other and the boundary substantially, i.e. it is valid only when the volume is large enough:  $M_i L \gg 1$  for all  $i$ . Note that if the particles involved in the calculation have no multiplicity labels, the transfer matrix is a scalar phase itself and can be directly substituted into Eqs. (4.2). Taking the logarithm of Eqs. (4.2) yields

$$2M_k L \sinh(\theta_k) - i \log \lambda_k^{(s)}(\theta_1, \dots, \theta_N) = 2\pi I_k \quad , \quad k = 1, \dots, N . \quad (4.3)$$

---

<sup>4</sup>For scalar particles, these equations appeared in [12].

where the  $I_k$  are integers that we call Bethe quantum numbers. In this way a given multi-particle state can be labeled by giving  $s$  and a set of integers  $I_1, \dots, I_N$  and this labeling is normally unique given a consistent choice of the branch of the logarithm. There are some exceptions when for given  $s$  and  $I_1, \dots, I_N$  Eqs. (4.3) admit more than one solution; such cases will be explicitly indicated below.

Note that in these considerations we neglected the contribution of vacuum polarization. Since, on dimensional grounds, we expect this contribution to behave as  $\mathcal{O}(\exp(-ML))$  for large  $L$ -s (with  $M$  being some characteristic mass scale), the polynomially decreasing, leading finite size corrections are indeed described by Eq.(4.3).

## 4.2 Some particular cases

Here we write down and analyze Eqs. (4.3) for some simple configurations that will play an important role in the sequel.

### 4.2.1 States containing a single scalar particle

For a state containing a single scalar particle of mass  $M$ , Eqs. (4.3) reduce to the single equation

$$2ML \sinh(\theta) - i \log R_L(\theta) - i \log R_R(\theta) = 2\pi I . \quad (4.4)$$

The energy of the state with respect to the vacuum can be written as

$$E(L) - E_0(L) = E_R + E_L + M \cosh \theta ,$$

where  $E_{R,L}$  denote the boundary energy of the left and right boundaries with respect to the boundary ground state (note that the boundary can also be in an excited state). One can easily express the function  $E(L) - E_0(L)$  in a parametric form using  $\theta$ .

Our studies show that for  $ML \ll 1$  Eqn. (4.4) always has a real solution irrespective of the choice of the quantum number  $I$ . However this may not be true for larger values of  $ML$ . Let us discuss the particular case  $I = 0$  and introduce the notation

$$\rho_{L,R} = i \frac{\partial}{\partial \theta} \log R_{L,R}(\theta) \Big|_{\theta=0} .$$

It is a generic property of reflection factors that  $i \log R_{L,R}(\theta)$  has a finite limit as  $\theta \rightarrow \pm\infty$ ; it also follows from unitarity that they are odd functions. Therefore the equation

$$2ML \sinh(\theta) = i \log R_L(\theta) + i \log R_R(\theta) \quad (4.5)$$

has a pair of nonzero solutions as long as

$$2ML < \rho_L + \rho_R .$$

Increasing  $L$ , these two solutions move towards the origin, which they reach at a finite volume

$$L_0 = \frac{1}{2M} (\rho_L + \rho_R) .$$

The question arises: what happens for volumes  $L > L_0$ ? If  $ML_0 \gg 1$  the Bethe-Yang equations should give a good approximation of the finite volume spectrum around this point. However, eigenvalues cannot simply disappear as the Hamiltonian we are concerned with is Hermitian. In fact, the spectrum is real and every eigenvalue is a continuous (even smooth) function of  $L$ . This leads us to the description of boundary bound states.

## 4.2.2 Description of boundary bound states in finite volume

Quite naturally, the two solutions of Eqn. (4.5) do not disappear, but continue their life as complex (eventually imaginary) solutions. Substituting  $\theta = iu$  into Eqn. (4.5) we obtain

$$2ML \sin(u) = \log R_L(iu) + \log R_R(iu) . \quad (4.6)$$

As reflection factors always take real values on the imaginary axis (as a result of analytic  $S$ -matrix theory) this is a real equation and it has a pair of real solutions for  $u$  exactly when  $L > L_0$ . The energy corresponding to this solution is

$$E(L) - E_0(L) = E_R + E_L + M \cos u .$$

This is smaller than  $E_R + E_L + M$  which means that this state cannot correspond to a real particle between the two boundaries.

The reflection factors  $R_L$  and  $R_R$  normally have poles on the imaginary axis. Let us denote the one which is closest to the origin by  $u^*$  and suppose it occurs in  $R_L$  only<sup>5</sup>. Then one has

$$u \rightarrow u^* \quad \text{as} \quad L \rightarrow \infty$$

and so

$$E(L = \infty) - E_0(L = \infty) = E_R + E_L + M \cos u^* .$$

Suppose also that  $u^*$  corresponds to a boundary bound state  $|B_L^*\rangle$  in the bootstrap, then the energy of such a state is

$$E_{L^*} = E_L + M \cos u^* .$$

It is then tempting to interpret the corresponding state as one without particles but in which the left boundary is excited to the state corresponding to the pole at  $u = u^*$ . Indeed our numerical data show complete consistency with this interpretation.

When the left and the right boundary conditions are identical (e.g both are Neumann), both reflection factors have a pole at  $u = u^*$ . One can then interpret the resulting ‘finite size state’ as one in which one of the boundaries is an excited one. This can be realized with two wave functions (as we have two identical boundaries) and we expect that the state described above corresponds to one of them. Note that in the above solution we always have  $u < u^*$ . The other one can be described (at least for large enough  $L$ ) by noting that there is going to be another solution  $u'$  to Eqn. (4.6) which satisfies  $u' > u^*$  and also approaches  $u^*$  for  $L \rightarrow \infty$ . It is clear, that, for finite  $L$ , the solution with  $u'$  has a lower energy than that of with  $u$ .

When  $L$  and  $R$  are not identical and the boundary state,  $|B_R\rangle$ , is not identical to the excited  $|B_L^*\rangle$  either, one again expects two wave functions for the system with no particles, so the two solutions that exist in this case too can be interpreted once again in this way. However, when  $|B_R\rangle = |B_L^*\rangle$  only one of the solutions can have an interpretation in terms of a real physical state. This shows that not necessarily all solutions of the Bethe-Yang equations (4.1) correspond to physical states. In fact, when  $u^*$  corresponds to a Coleman-Thun pole, we do not even expect the  $I = 0$  state to appear in the spectrum, since then we would have some state for  $L < L_0$  that does not have any physical continuation to  $L_0 < L$ .

There is a generalization of this line of thought to other poles that are further away from the origin in the physical strip  $0 < u < \pi/2$ . We cannot expect these to be realized in

---

<sup>5</sup>We meet this situation e.g. in sine-Gordon model with  $\phi|_R = 0$  (special Dirichlet) and  $\partial_x \phi|_L = 0$  (Neumann) b.c.s.

an analytic continuation from a state with real rapidities, since any such continuation goes through the origin  $u = \theta = 0$  and necessarily runs into the pole closest to 0. However, we can calculate solutions of Eqn. (4.6) around any such pole (of course one cannot go too far from the given pole since one then generally runs into the domain of some other singularity of the reflection factor). For large enough  $L$ , such a solution exists and generalizing the above scheme one expects that it can describe the leading finite size behaviour of some excited boundary state in finite volume if the pole in question participates in the bootstrap. Once again, Coleman-Thun poles can have no such corresponding state in the finite size spectrum.

A given excited boundary state may arise from different reflection factors as a pole (e.g. in SGN the state  $|n\rangle$  arises from both the soliton and the  $B^n$  reflections) and therefore a further possibility is that it can be described in finite volume in more than one ways.

Later in this paper we show that all the above considerations are well confirmed by our numerical studies. We wish to remark that similar ideas to describe bound states appeared in [13] for the bulk and in [14] for the boundary case.

### 4.2.3 States with two scalar particles

In the case of two scalar particles of mass  $M_1$  and  $M_2$ , the Bethe-Yang equations take the form

$$\begin{aligned} 2M_1 L \sinh \theta_1 - i \log R_L^{(1)}(\theta_1) - i \log R_R^{(1)}(\theta_1) - i \log S^{(12)}(\theta_1 - \theta_2) \\ - i \log S^{(12)}(\theta_1 + \theta_2) = 2\pi I_1, \\ 2M_2 L \sinh \theta_2 - i \log R_L^{(2)}(\theta_2) - i \log R_R^{(2)}(\theta_2) - i \log S^{(12)}(\theta_2 - \theta_1) \\ - i \log S^{(12)}(\theta_2 + \theta_1) = 2\pi I_2, \\ E(L) - E_0(L) = E_R + E_L + M_1 \cosh \theta_1 + M_2 \cosh \theta_2. \end{aligned} \quad (4.7)$$

In this case, these equations can only be solved by numerical iteration. One can also continue these equations to imaginary value of one (or both) of the rapidities. Using that the reflection factors are real for purely imaginary rapidities together with unitarity and real analyticity of the bulk  $S$  matrix one can show (just as for the one-particle case) that the resulting equations are consistent and the energy of the solutions is always real. Consider e.g. the Bethe Yang equations for  $B^n$ - $B^m$  with rapidities  $iu$  and  $\theta_2$  respectively, which, before taking the logarithm, can be written as

$$\begin{aligned} R_L^{(n)}(iu) R_R^{(n)}(iu) |S^{(n,m)}(\theta_2 + iu)|^2 e^{-2m_n l \sin u} = 1, \quad l = ML, \\ R_L^{(m)}(\theta_2) R_R^{(m)}(\theta_2) \frac{S^{(n,m)}(\theta_2 + iu)}{S^{(n,m)}(\theta_2 + iu)^*} e^{i2m_m l \sinh \theta_2} = 1, \quad m_{n,m} = \frac{M_{n,m}}{M}. \end{aligned} \quad (4.8)$$

The first is a real equation with real entries, and each factor on the left hand side of the second equation is of unit modulus. Thus, when taking the logarithms, for the complete system there is only one quantum number,  $I_m$ , coming from the second equation. Two particle states with one rapidity being imaginary are important, as one can argue that the best way to describe one particle states moving between an excited and a ground state boundaries is to use (4.7-4.8) with *ground state* reflection factors and an imaginary rapidity tuned into the vicinity of a pole corresponding to the excited state. When both rapidities are imaginary, the solutions of (4.7) describe zero particle states with excited boundaries.



## 5 Truncated Conformal Space Approach (TCSA) for the boundary sine-Gordon model

Here we describe the Hamiltonian of boundary sine-Gordon model (BSG) living on the line segment  $0 \leq x \leq L$  as that of a bulk and boundary perturbed free boson with suitable boundary conditions. This is the starting point of the TCSA analysis.

The basic idea of TCSA is to describe certain  $2d$  models as relevant perturbations of their ultraviolet limiting CFT-s [8]. If we consider boundary field theories, then the CFT-s in the ultraviolet are in fact boundary CFT-s. The use of TCSA to investigate boundary theories was advocated in [14, 15].

As the bulk SG can be successfully described as a perturbation of the  $c = 1$  free boson [16], it is natural to expect, that the various BSG models are appropriate perturbations of  $c = 1$  theories with Neumann or Dirichlet boundary conditions. Therefore we take the strip  $0 \leq x \leq L$  and consider the following perturbations of the models described in detail in Appendix C:

$$S = \int_{-\infty}^{\infty} \int_0^L \left( \frac{1}{8\pi} \partial_\mu \Phi \partial^\mu \Phi + \mu \cos(\beta \Phi) \right) dx dt + \int_{-\infty}^{\infty} \left( M_0 \left[ \cos \left( \frac{\beta}{2} (\Phi_B - \phi_0) \right) - 1 \right] + M_L \left[ \cos \left( \frac{\beta}{2} (\Phi_B - \phi_L) \right) - 1 \right] \right) dt .$$

Here, for finite  $M$ 's, Neumann boundary conditions are imposed in the underlying  $c = 1$  theory on the boundaries, while if any of the  $M$ -s is infinite then the corresponding term is absent and the boundary condition in the underlying conformal theory on that boundary is Dirichlet. We can rewrite the Hamiltonian of the system in terms of the variables associated to the plane using the map  $(x, it) = \xi \rightarrow z = e^{i\frac{\pi}{L}\xi}$ , and by changing the integration variable we have

$$H = H_{CFT} + \frac{\mu}{2} \left( \frac{\pi}{L} \right)^{2h_\beta - 1} \int_0^\pi (V_\beta(e^{i\theta}, e^{-i\theta}) + V_{-\beta}(e^{i\theta}, e^{-i\theta})) d\theta + \frac{M_0}{2} \left( \frac{\pi}{L} \right)^{h_\beta} \left( e^{-i\frac{\beta}{2}\phi_0} \Psi_{\frac{\beta}{2}}(1) + e^{i\frac{\beta}{2}\phi_0} \Psi_{-\frac{\beta}{2}}(1) \right) + \frac{M_L}{2} \left( \frac{\pi}{L} \right)^{h_\beta} \left( e^{-i\frac{\beta}{2}\phi_L} \Psi_{\frac{\beta}{2}}(-1) + e^{i\frac{\beta}{2}\phi_L} \Psi_{-\frac{\beta}{2}}(-1) \right) . \quad (5.1)$$

Now the computation of the matrix elements of the bulk and boundary vertex operators  $V_{\pm\beta}$  and  $\Psi_{\pm\beta/2}$  (with conformal dimension  $h_\beta$ ) between the vectors of the appropriate conformal Hilbert spaces is straightforward. Also the integrals can be calculated explicitly. Truncating the Hilbert space at a certain conformal energy level  $E_{\text{cut}}$  (which is nothing but the eigenvalue of the zeroth Virasoro generator) and diagonalizing the Hamiltonian numerically we arrive at the TCSA method.

The TCSA Hamiltonian for BSG with Neumann boundary conditions at both ends is obtained from (5.1) by setting  $M_0 = M_L = 0$  and using (C.5), (C.6) with  $n = 1$ ,  $r = \sqrt{4\pi}/\beta$  for  $H_{CFT}$  and  $V_\beta$ , while the TCSA Hamiltonian for BSG with mixed boundary conditions is obtained by setting  $M_0 = M_L = 0$  and using (C.9) and (C.10) with the same  $n$  and  $r$  for  $H_{CFT}$  and  $V_\beta$ .

We choose our units in terms of the soliton mass  $M$ . The bulk coupling  $\mu$  is related to  $M$  by

$$\mu = \kappa(\beta) M^{2-2h_\beta}, \quad h_\beta = \frac{\beta^2}{8\pi}, \quad (5.2)$$

where  $\kappa(\beta)$  is a dimensionless constant. In the bulk SG, from TBA considerations, the exact form of  $\kappa(\beta)$  was obtained in [17], and we use the same form also here in BSG. Once we expressed  $\mu$ , the Hamiltonian, (5.1), can be made dimensionless  $h = H/M$ , depending only on the dimensionless volume parameter  $l = ML$  and  $\beta$  (in the general case it also depends on  $M_{0,L}/M$  and  $\phi_{0,L}$ ).

## 6 TCSA analysis of SGN in finite volume

In this section we review the TCSA analysis of the BSG with Neumann boundary condition. The aim of this investigation is twofold: first we want to verify the various reflection factors and the boundary spectrum obtained from the bootstrap procedure, and second we want to obtain further information about the finite volume behaviour of SGN. We consider in some detail the questions of the ground state and the associated boundary energies, the low lying one particle states and their reflections on the ground state wall and finally the new states predicted by the bootstrap.

In SGN, as  $\mathbf{C}$  symmetry persists, there are two sectors, the  $\mathbf{C} = 1$  even and the  $\mathbf{C} = -1$  odd ones. The bulk breathers naturally belong to one of them, as the  $\mathbf{C}$  parity of the  $n$ -th breather is  $(-1)^n$ . However, since solitons and anti solitons can reflect into themselves as well as into their charge conjugate partners, solitonic one particle states (i.e. states, whose energy and momentum are related by  $E = \sqrt{P^2 + M^2}$  where  $M$  is the soliton mass) are there in both sectors. The ground state is in the even sector, while we expect  $|1\rangle$  to be of the lowest energy one in the odd sector (at least for  $p < 1/2$ , which is true for all the cases investigated by us).

If at both ends of the strip Neumann boundary condition is imposed (NN case), then sometimes we have to face the problem of identifying the TCSA lines (states) corresponding to the symmetric/antisymmetric combinations of some identical excited states of the identical boundaries, as described in section 4. Therefore in the NN case the finite volume spectrum and consequently the TCSA line sequences are more complex than the ‘naive’ one derived by the bootstrap procedure in section 3. To avoid this complication when ‘verifying’ the Neumann spectrum we consider a system, where Dirichlet boundary condition with  $\phi_0 = 0$  is imposed on one of the boundaries, while keeping the Neumann one at the other (DN case). Since this mixed boundary condition is also  $\mathbf{C}$  symmetric we do not lose the presence of even and odd sectors on the one hand, while, on the other, we can be sure, that any boundary bound state (BBS) found in this case can be attributed to the Neumann end of the strip, as this Dirichlet boundary condition has no bound states [4].

As charge conjugation acts on the fundamental scalar field by  $\Phi \mapsto -\Phi$ , it is straightforward to implement the projection onto the even and odd sectors in the conformal Hilbert spaces used in TCSA. This projection has two beneficial effects: on the one hand it effectively halves the number of states below  $E_{\text{cut}}$ , thus it drastically reduces the time needed to obtain the complete TCSA spectrum, and on the other the separate spectra of the even and odd sectors are less complex and therefore easier to study than the combined one.

In our numerical studies  $E_{\text{cut}}$  varied between 16 and 25, and this resulted in  $4.5 \times 10^3$  -  $8 \times 10^3$  conformal states per sectors. In the DN case the number of states below  $E_{\text{cut}}$  is independent of  $p$ , while in the NN case it depends sensitively on it.

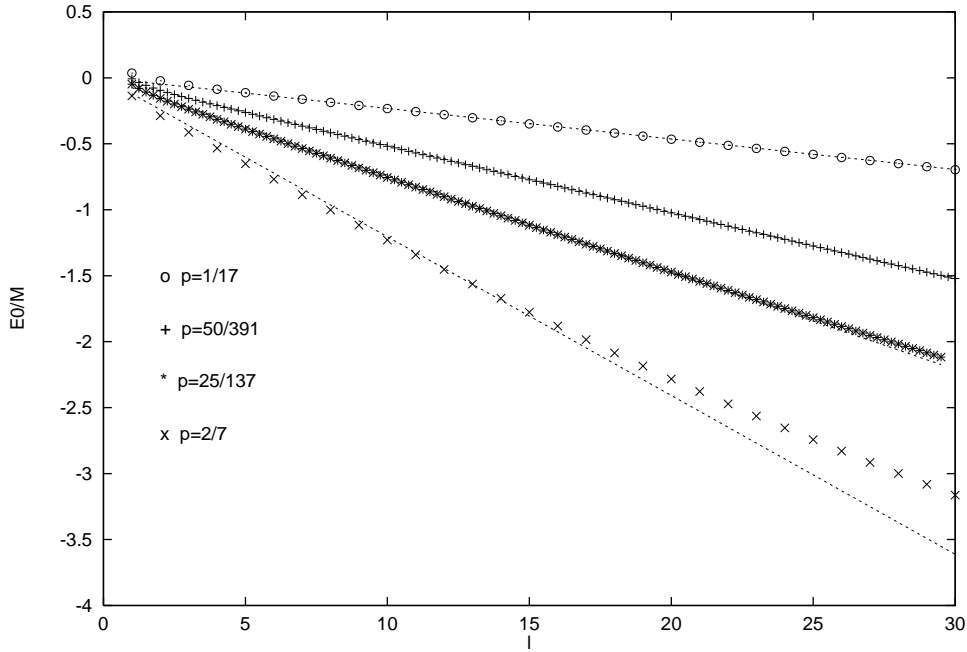


Figure 6.1: Ground state energy versus  $l$  in the DN case at various  $p$ -s. The slope of the dashed lines is  $-\frac{1}{4} \tan(\frac{p\pi}{2})$ .

## 6.1 Ground state and boundary energy

In any boundary field theory in finite volume, for large enough  $L$ -s, we expect on general physical grounds, that the volume dependence of the ground state energy can be written as

$$E_0(L) = \epsilon_0 L + \mathcal{E}_L + \mathcal{E}_R, \quad (6.1)$$

where  $\epsilon_0$  is the ground state energy density and  $\mathcal{E}_{L,R}$  are the ground state boundary energies associated to the left and right ends of the strip. In the BSG model one can argue that  $\epsilon_0$  is nothing but the well known bulk energy constant,  $-\frac{M^2}{4} \tan(\frac{p\pi}{2})$ , of the bulk SG theory. In BSG with Dirichlet boundary conditions, LeClair et al. [18] were able to obtain  $\mathcal{E}_{\text{Dir}}$  from TBA, at least for those values of  $p$  when not only the boundary but also the bulk scatterings become diagonal. The case of Neumann boundary condition is more complicated as there is no  $p$  where the boundary scatterings would become diagonal.

Nevertheless using TCSA, we can get information on  $\mathcal{E}_{\text{Neu}}$ . To this end we determined  $E_0(l)/M$  ( $M$  is the soliton mass and  $l = ML$  is the dimensionless volume parameter) from our TCSA data at various values of  $p$  both in the (DN) and in the (NN) cases; the results are shown on Figs.(6.1-6.2) These figures show in a convincing way that in these BSG models  $\epsilon_0$  is indeed the expected one. Interestingly the (DN) data for  $E_0(l)/M$  are consistent with a straight line passing through the origin; i.e. with  $\mathcal{E}_{\text{Neu}}(p) = -\mathcal{E}_{\text{Dir}}(p, \phi_0 = 0)$ . Since from ref.[18] we know  $\mathcal{E}_{\text{Dir}}$  analytically, using the (DN) data we have a prediction for  $E_0(l)/M$  in the (NN) case: a straight line with slope parameter  $-\frac{1}{4} \tan(\frac{p\pi}{2})$  and intersection

$$2 \frac{\mathcal{E}_{\text{Neu}}}{M} = -\frac{1}{2} \left( 1 - \frac{2}{\cos(\frac{p\pi}{2})} + \cot(\frac{\pi(p+1)}{4}) \right). \quad (6.2)$$

Fig.(6.2) shows that this prediction is consistent with our (NN) data.

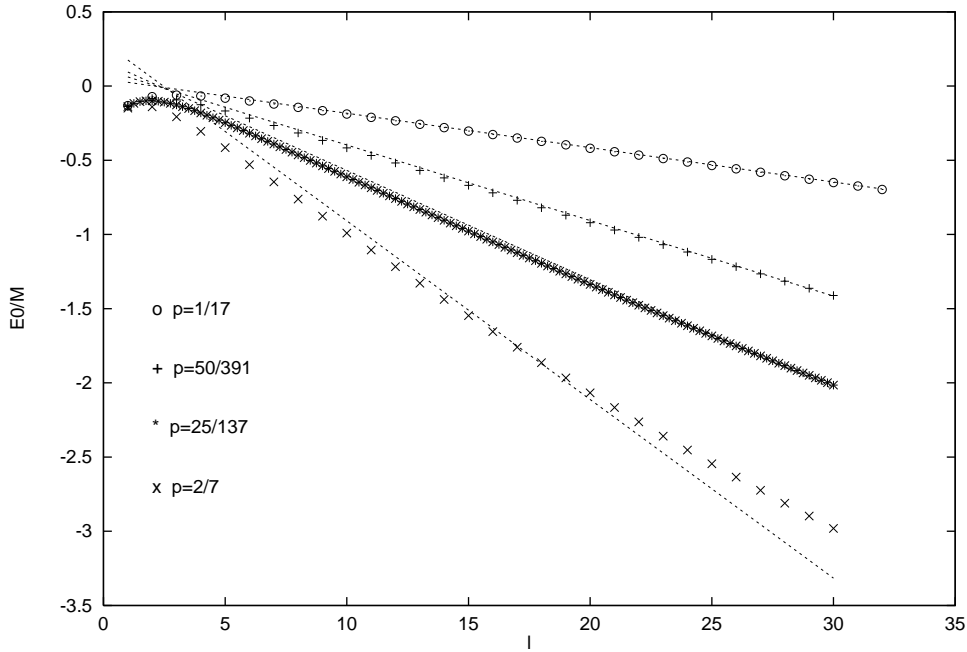


Figure 6.2: Ground state energy versus  $l$  in the NN case at various  $p$ -s. The slope of the dashed lines is the same as on Fig.(6.1), but their intersection is given by Eq.(6.2).

## 6.2 Low lying one particle lines, reflections on the ground state wall

Next we summarize what we can learn about the Neumann spectrum by studying the lowest lying one particle states.

### 6.2.1 Breather lines

Using the formalism developed in section 4 it is straightforward to express in parametric form the Bethe - Yang (BY) lines corresponding to the various breathers moving between ground state walls at the ends of the strip<sup>6</sup> :

$$(E(L), L) = (M_n \cosh \theta, (2\pi I_n + i \log R_L^{(n)}(\theta) + i \log R_R^{(n)}(\theta))/(2M_n \sinh \theta)) . \quad (6.3)$$

Here  $E(L)$  is the energy of the  $n$ -th breather above the ground state,  $\theta$  (the parameter of the line) is the rapidity of  $B^n$  (which, therefore, necessarily must be real and non negative), and  $M_n$  is the mass of  $B^n$ .  $I_n$  is the quantum number characterizing the line; if  $R_L^{(n)}(0)R_R^{(n)}(0) = 1$  then  $I_n$  is integer, while if  $R_L^{(n)}(0)R_R^{(n)}(0) = -1$  then  $I_n$  is half integer. (If  $R_L^{(n)}(\theta) = R_R^{(n)}(\theta)$  as in the (NN) case, then only the first possibility appears, the second happens e.g. in the (DN) case for the  $\mathbf{C}$  even breathers).

The perfect agreement between the TCSA data and the predictions coming from (6.3) for  $B^1$ ,  $B^2$  and  $B^3$  with  $I_n > 0$  in both the (DN) and the (NN) cases - as summarized in Figs.(6.3-6.4) - gives convincing evidence for the correctness of the reflection factors given in [3].<sup>7</sup>

<sup>6</sup>Among the breather lines these are of the lowest in energy above the ground state.

<sup>7</sup>On Figs.(6.3-6.6) the dimensionless energy levels above the ground state are plotted against  $l$ . On all plots the continuous lines are the interpolated TCSA data and the various symbols mark the data corresponding to the various BY lines. Some of the higher TCSA lines appear to have been broken, the apparent turning

Using the parametric form of  $L(\theta)$  given in (6.3) together with the limits

$$\lim_{\theta \rightarrow 0} R_L^{(n)}(\theta)R_R^{(n)}(\theta) = \pm 1, \quad \lim_{\theta \rightarrow \infty} |\log R_L^{(n)}(\theta)R_R^{(n)}(\theta)| < \infty$$

it is straightforward to show that for  $I_n > 0$  the range of  $L(\theta)$  runs from zero to infinity, as  $\theta$  decreases from infinity to zero (i.e. as we move from the UV to the IR). However, as it was explained in section 4, in the case of  $I_n = 0$  there is a maximal value of  $L_0$  beyond which we can not go keeping  $\theta$  real. We can see this phenomenon on the  $I_n = 0$  lines on Figs.(6.3-6.4). Interestingly, there are TCSA lines on Figs.(6.3-6.4) which, below a maximal  $L$ , can be described well by breather (BY) lines with *negative* quantum numbers like the  $B^2$  line with  $I_2 = -1/2$  or the  $B^3$  line with  $I_3 = -1$ . The essential difference between the  $L(\theta)$  functions with  $I_n = 0$  and the ones with  $I_n < 0$  is that while the former ones reach their maximal value at  $\theta = 0$ , the latter ones do this at some positive  $\theta$ . Therefore, while in the former case the BY lines can be continued by going to purely imaginary rapidity, we can not do this in the latter cases. As illustrated on Figs.(6.3-6.5) this continuation describes the TCSA data very well as  $u = -i\theta$  moves from zero towards the first singularity in the reflection factors, if this first singularity corresponds to a bound state pole in bootstrap: see the  $B^1$  lines ending in the  $e_1$  bound state in both the (DN) and the (NN) cases.

These Figures also show that the idea put forward in section 4 to describe (at least for large enough  $L$ -s) the TCSA lines corresponding to BBS by appropriate one particle (here breather) BY lines with purely imaginary rapidities (independently whether they are obtained from continuation through  $\theta = 0$  or not) works indeed. At this point the comparison of the DN and NN spectra is very instructive: while in the DN cases there are only single lines that descend to  $e_1$  or  $e_2$  from above for large  $L$ -s, in the NN cases one can see both an increasing and a decreasing line tending to  $e_1$  and  $e_2$ . In the latter case these nearly degenerate TCSA states may be interpreted as the symmetric and antisymmetric wave functions in which one of the identical (and hence indistinguishable) boundaries is in an excited state and the other one is in the ground state. For large enough  $L$ -s the volume dependence of the nearly degenerate energies is well described by BY lines with purely imaginary rapidities just above or just below the values corresponding to  $e_1$  or  $e_2$ .

On the last two plots in Fig.(6.5) we also exhibit the appearance of the  $|3\rangle$  state in an expected way. For  $p = 25/137$  (when the state  $|3\rangle$  is absent) the BY line marked by the o-s is a solitonic line with  $N = 1$  extending to infinity, while for  $p = 50/391$  (when  $|3\rangle$  is already present) it is a solitonic line with  $N = 0$ , ending at a maximal  $l$ . In this latter case the TCSA data in the continuation of this BY line are correctly described by the x-s, which are the data from the BY line of the third breather with imaginary rapidity just below  $u_3$ .

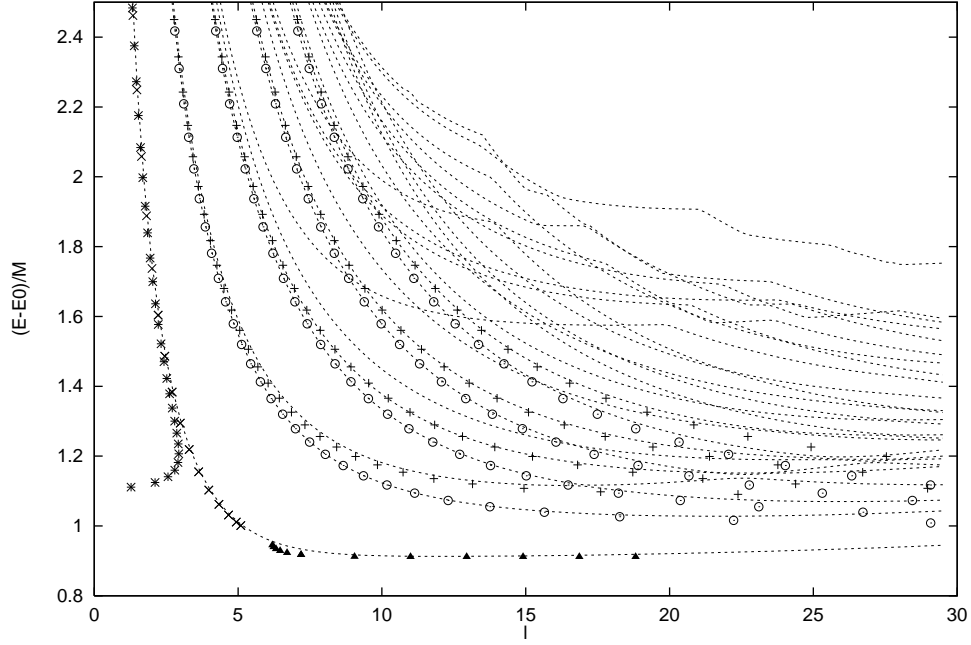
## 6.2.2 Soliton lines

As mentioned in the introduction to this section in the description of solitonic one particle states we have to face the problem of non diagonal reflections. In the  $\mathbf{C}$  symmetric case (i.e. when  $s \leftrightarrow \bar{s}$  is a symmetry) the one particle soliton anti soliton transfer matrix is  $2 \times 2$ , and the Bethe Yang equations using the eigenvalues of this matrix take the form

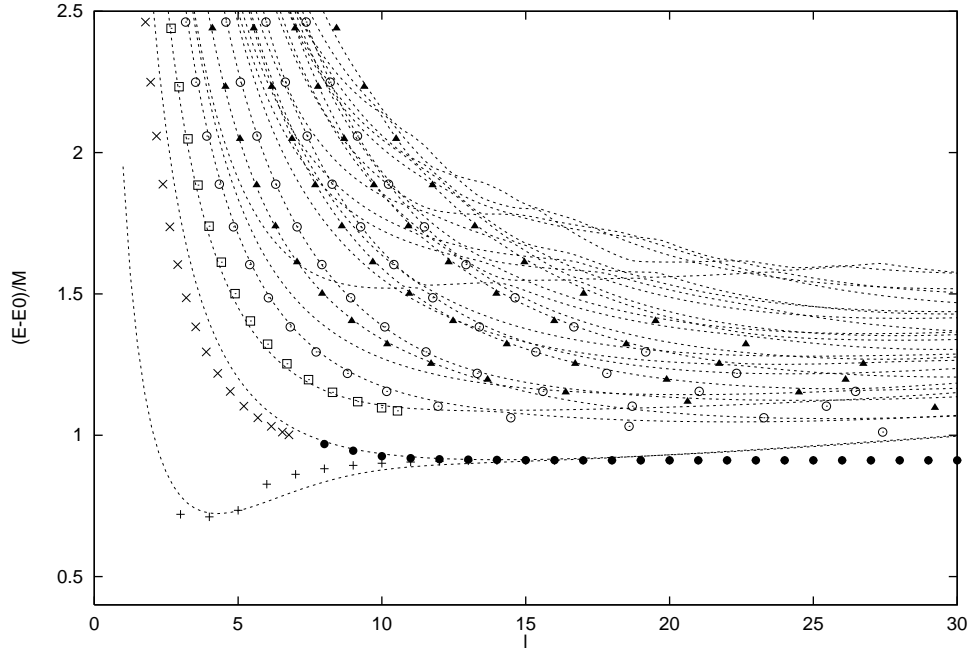
$$1 = e^{i2ML \sinh \theta} (P_L(\theta) \pm Q_L(\theta))(P_R(\theta) \pm Q_R(\theta)) , \quad (6.4)$$

---

points are in fact level crossings with the other line not shown. This happens because our numerical routine, instead of giving the eigenvalues of the Hamiltonian in increasing order at each value of  $l$ , fixes their order at a particular small  $l$  and follows them – keeping their order – according to some criteria as  $l$  is changing to higher values.



DN spectrum: + and \* denote the  $B^2$  lines with  $I_2 = \frac{1}{2} \dots \frac{7}{2}$  and  $-\frac{1}{2}$ ,  
 o and x the soliton lines with  $N = 1 \dots 4$  and 0,  
 the full triangles the  $B^2$  line with imaginary rapidity.



NN spectrum: the full triangles and empty boxes are the  $B^2$  lines with  $I_2 = 1 \dots 4$  and 0,  
 o and x the soliton lines with  $N = 1 \dots 4$  and 0,  
 the  $\bullet$  and the + the  $B^2$  lines with imaginary rapidities just below and above  $u_2$ .

Figure 6.3: TCSA data and soliton/breather Bethe Yang lines in the  $\mathbf{C}$  even sectors with  $p = 25/137$ .

where, in the  $\mathbf{C}$  even/odd sectors the upper/lower signs apply, and  $P_{L,R}(\theta)$  ( $Q_{L,R}(\theta)$ ) denote the soliton soliton (soliton anti soliton) reflection factors on the ground state left and right boundaries. In the (NN) case these equations simplify to

$$1 = e^{i2l \sinh \theta} (P(\theta) \pm Q(\theta))^2, \quad l = ML, \quad (6.5)$$

while in the (DN) case - when on the Dirichlet wall  $Q$  vanishes - to

$$1 = e^{i2l \sinh \theta} (P(\theta) \pm Q(\theta))P_D(\theta). \quad (6.6)$$

(Here  $P_D$  is the  $\xi = 0$  case of the soliton reflection factor in BSG with Dirichlet boundary conditions:  $P_D(\theta) = P^{(+)}(\theta)|_{\xi=0}$  of ref. [4]). Using the infinite product form of  $P$ ,  $Q$  and  $P_D$  it is straightforward to verify, that the expressions multiplying  $e^{i2l \sinh \theta}$  in Eq. (6.5-6.6) are indeed pure phases - at least for  $0 \leq \theta \leq \infty$  - thus these equations make sense.

The infinite product representation is not very useful when we compare BY lines coming from Eq. (6.5-6.6) to the TCSA data. Therefore, using the well known integral representation for the logarithm of the Gamma function, we recast  $l(\theta)$  such that the parametric form of the solitonic BY lines looks like (with  $E(l)/M$  denoting the energy above the ground state):

$$(E(l)/M, l) = (\cosh \theta, l(\theta)), \quad (6.7)$$

where

$$l(\theta) = \frac{N\pi + \mathbf{a}i \log r_{\pm} + I(p, \theta)}{\sinh \theta}, \quad (6.8)$$

with

$$I(p, \theta) = \int_0^{\infty} \frac{dy}{y} \sin\left(\frac{2\theta y}{\pi}\right) \left( \frac{2 \sinh(3y/2) \sinh([1-p]y/2)}{\sinh(py/2) \sinh(2y)} + \frac{\mathbf{a} \sinh(py) - \sinh(y)}{\cosh(y) \sinh(py)} \right), \quad (6.9)$$

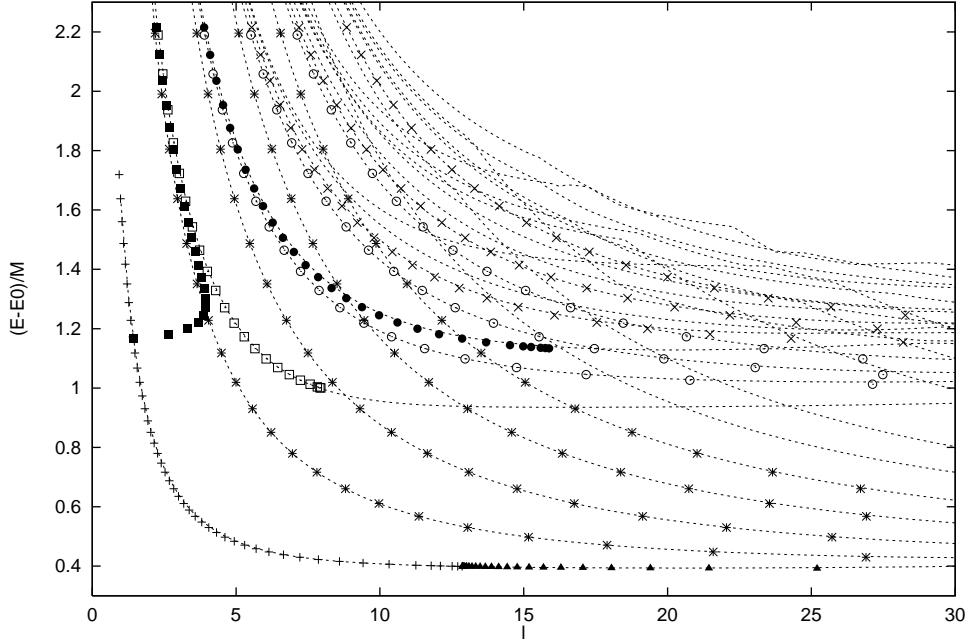
and

$$r_+ = \frac{\sin\left(\frac{\pi}{4p} - i\frac{\theta}{2p}\right)}{\sin\left(\frac{\pi}{4p} + i\frac{\theta}{2p}\right)}, \quad r_- = \frac{\cos\left(\frac{\pi}{4p} - i\frac{\theta}{2p}\right)}{\cos\left(\frac{\pi}{4p} + i\frac{\theta}{2p}\right)}, \quad (6.10)$$

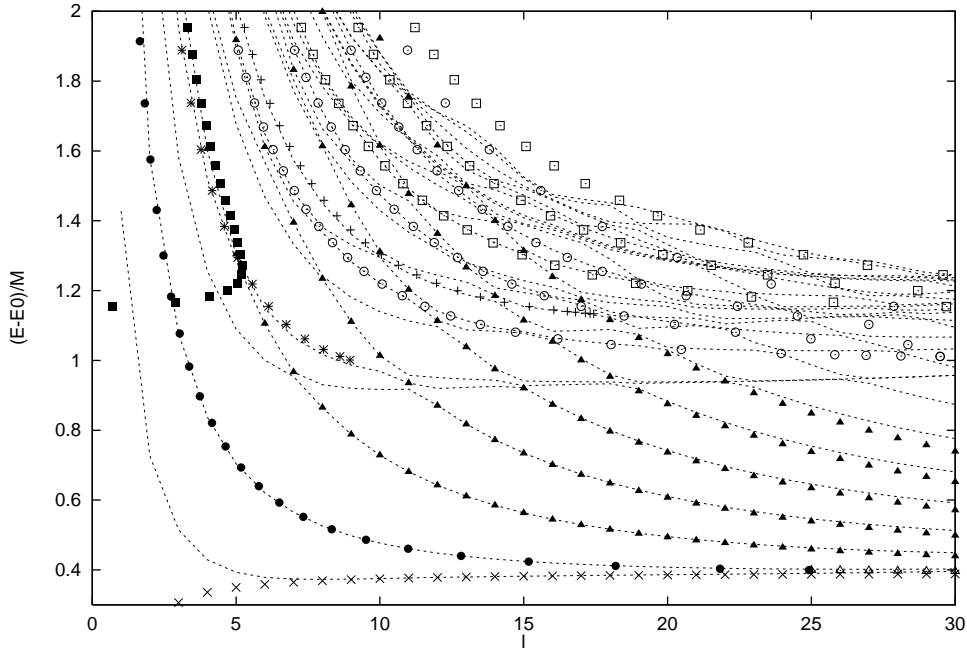
in the  $\mathbf{C}$  even/ $\mathbf{C}$  odd sectors. Here the parameter  $\mathbf{a}$  is one,  $\mathbf{a} = 1$ , in the (NN) case and is one half,  $\mathbf{a} = 1/2$ , in the (DN) case; the quantum number  $N$ , characterizing the BY line, is a non negative integer in all sectors and all cases and -as before -  $\theta$  is both the parameter of the line and the rapidity of the solitonic particle. (Although this representation of the solitonic BY lines works for real rapidities only, one can show that all the “boundary dependent” poles at  $\theta = iu$  come from  $\log r_{\pm}$ , in fact from the set of poles,  $\theta = i(\frac{\pi}{2} - kp\pi)$ ,  $r_+$  has poles for  $k = 2N$  while  $r_-$  for  $k = 2N + 1$ ).

On Figs.(6.3-6.4) we demonstrate the excellent agreement between the TCSA data and the BY lines given by (6.7-6.10) with  $N > 0$  in both the  $\mathbf{C}$  even and the  $\mathbf{C}$  odd sectors of the (DN) and (NN) cases. This agreement gives a strong evidence for the correctness of the solitonic reflection factors given in [1].

Note that in some cases we have TCSA lines that below a maximal  $L$  can be described well by solitonic BY lines with zero quantum number,  $N = 0$ . The continuation of these BY lines to imaginary rapidities - that worked for the breather lines - is hampered by the fact, that in all the cases investigated, the pole in  $(P \pm Q)^2$  or  $(P \pm Q)P_D$  nearest to the origin turned out to be a Coleman-Thun pole. Therefore the solitonic BY lines continued to imaginary rapidities deviate from the TCSA data.



DN spectrum: \* and + denote the  $B^1$  lines with  $I_1 = 1 \dots 4$  and 0,  $\circ$  and the empty boxes the soliton lines with  $N = 1 \dots 3$  and 0, the full triangles the  $B^1$  line with imaginary rapidity, the x,  $\bullet$ , and the full boxes the  $B^3$  lines with  $I_3 = 1 \dots 3, 0$ , and  $-1$ .



NN spectrum: full triangles and  $\bullet$  denote the  $B^1$  lines with  $I_1 = 1 \dots 5$  and 0,  $\circ$  and \* the soliton lines with  $N = 1 \dots 4$  and 0, x and  $\Delta$  the  $B^1$  lines with imaginary rapidities just above and below  $u_1$ , the empty and full boxes and + the  $B^3$  lines with  $I_3 = 1 \dots 3, -1$ , and 0.

Figure 6.4: TCSA data and soliton/breather Bethe Yang lines in the  $\mathbf{C}$  odd sectors with  $p = 50/391$ .



### 6.3 New boundary bound states and reflections on excited walls

The most interesting application of TCSA is to find evidence for the existence of the new BBS-s predicted by the bootstrap and check the correctness of the ‘excited’ reflection factors, i.e. the ones describing the scattering of breathers/solitons on the wall in an excited state. In this inquiry it is very helpful to analyze the DN spectra: if, e.g. we find a TCSA line (state) with asymptotic (large  $l$ ) energy  $e_1 + e_2$  in the DN spectrum, then we can be sure that it indeed corresponds to the  $|1, 2\rangle$  state of the Neumann boundary. (Note that in the NN case there are more states having this asymptotics, as the energy of the configurations, when one of the Neumann boundaries is in the  $|1\rangle$  state and the other is in the  $|2\rangle$  state, also tends to  $e_1 + e_2$ ).

The state  $|1, 2\rangle$  can be generated by the third breather, furthermore, the corresponding pole at  $u_1$  is the one nearest to the origin in the third breather’s reflection factor. Therefore it is expected that the state  $|1, 2\rangle$  becomes visible as the imaginary continuation of a  $B^3$  BY line with  $I_3 = 0$ . We collected the evidence for the existence of  $|1, 2\rangle$  on fig.(6.5). On all three plots the continuous lines are the interpolated TCSA data, the +-s and the empty boxes denote the BY line of  $B^1$  and  $B^3$  with  $I_{1,3} = 0$  respectively, while the full triangles and the \*-s denote the continuations of these lines to purely imaginary rapidities with  $u$  ranging from zero to  $u_1$ . Note, that for  $p = 2/7$ , when, according to bootstrap considerations, there is no  $|1, 2\rangle$  state and the imaginary continuation of the  $B^3$  BY line should run into a Coleman - Thun pole, the BY line indeed departs from the TCSA data, (which, in this case are well described by a  $B^2B^1$  BY line where the second breather’s rapidity is imaginary and the first breather’s quantum number is  $I_1 = 1$ , the data corresponding to this line are given by the ●-s). On the other hand, when  $p$  is such that  $|1, 2\rangle$  should exist, we see that the imaginary continuation of the third breather’s BY line describes the TCSA data just as well as that of the first breather’s line, which runs into  $e_1$ .

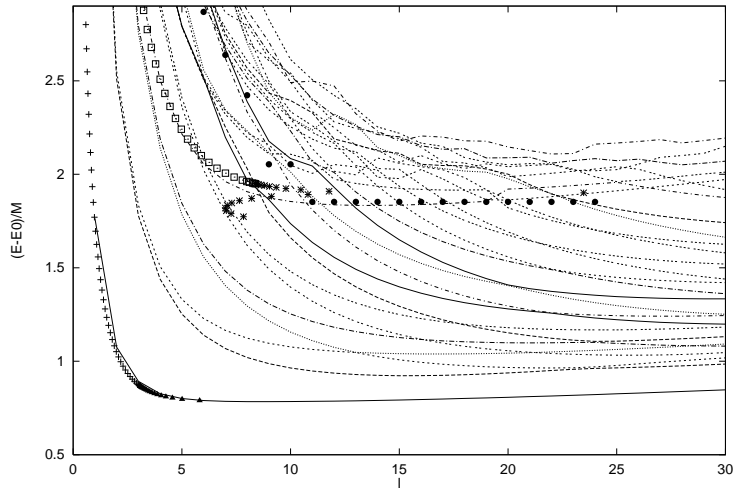
Further evidence for the existence of a new state predicted by the bootstrap is given on Fig.(6.6), where we exhibit a single TCSA line descending to  $e_1 + e_3$ . In the light of what we said above this indicates the existence of the boundary bound state  $|1, 3\rangle$ . (The horizontal lines corresponding to  $m_4 = M_4/M$  and the dimensionless  $e_1 + e_3$  are drawn to guide the reader’s eye to distinguish this line from the real fourth breather’s BY lines lying above  $m_4$ .) This state corresponds to the pole at  $u_2$  in the fourth breather’s reflection factor on the ground state boundary. Therefore, above a certain minimal  $l$ , the TCSA data in this line can certainly be described as the BY line of  $B^{(4)}$  with imaginary rapidity below  $u_2$ , but, since this reflection factor also has a pole at  $u_1$ , can not be obtained as the analytical continuation of a BY line through  $\theta = 0$ .

The bootstrap procedure gave not only the spectrum of the BBS but also the reflection factors describing the scatterings of the various breathers/solitons on excited boundaries. On Fig.(6.6) we also confirm the correctness of these new reflection factors.

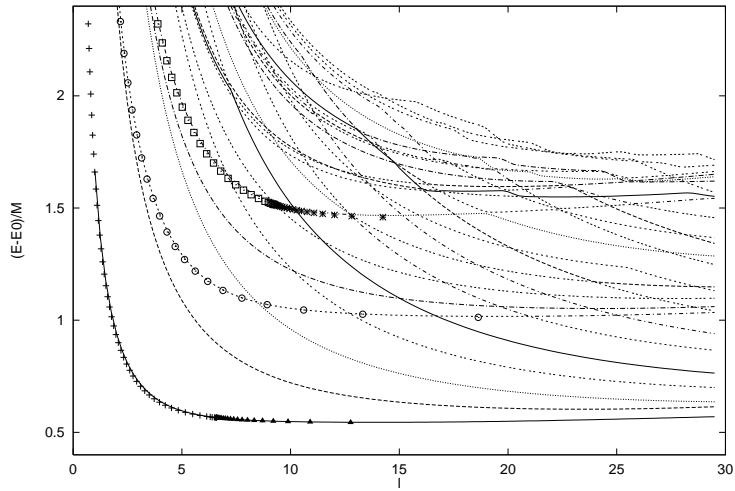
There are two ways one can describe the scattering of a breather, ( $B^n$  say), on an excited boundary  $|k\rangle$ . The first is to use a BY line (“excited” BY line) following from Eq.(4.4)

$$(E(L), L) = (e_k + M_n \cosh \theta, (2\pi I_n + i \log R_L^{(n)}(\theta) + i \log R_R^{(n)}(\theta))/(2M_n \sinh \theta)) , \quad (6.11)$$

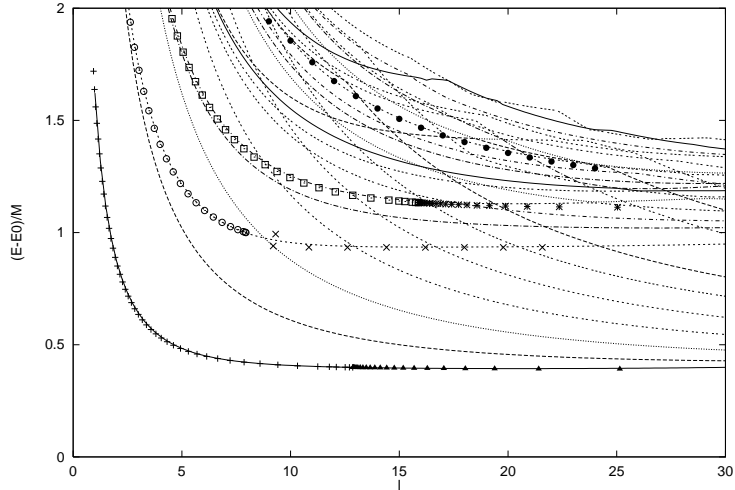
where  $R_R^{(n)}$  or  $R_L^{(n)}$  now corresponds to the appropriate  $R_{|k\rangle}^{(n)}$ , and the energy above the ground state is given by  $e_k + M_n \cosh \theta$ . This description, however, ignores the fact, that, in finite volume  $L$ , even in the absence of the moving  $B^n$ , the energy of the state  $|k\rangle$  only asymptotically coincides with  $e_k$ . To remedy this we may try to use a two particle BY line, where ground state reflection factors appear, but one of the particles moves with imaginary rapidity, (which



$p = 2/7$ , no  $|1, 2\rangle$  state exists



$p = 25/137$ , the  $|1, 2\rangle$  state exists



$p = 50/391$ , the  $|1, 2\rangle$  state exists

Figure 6.5: Evidence for the existence of the  $|1, 2\rangle$  state from three  $C = -1$  DN spectra.

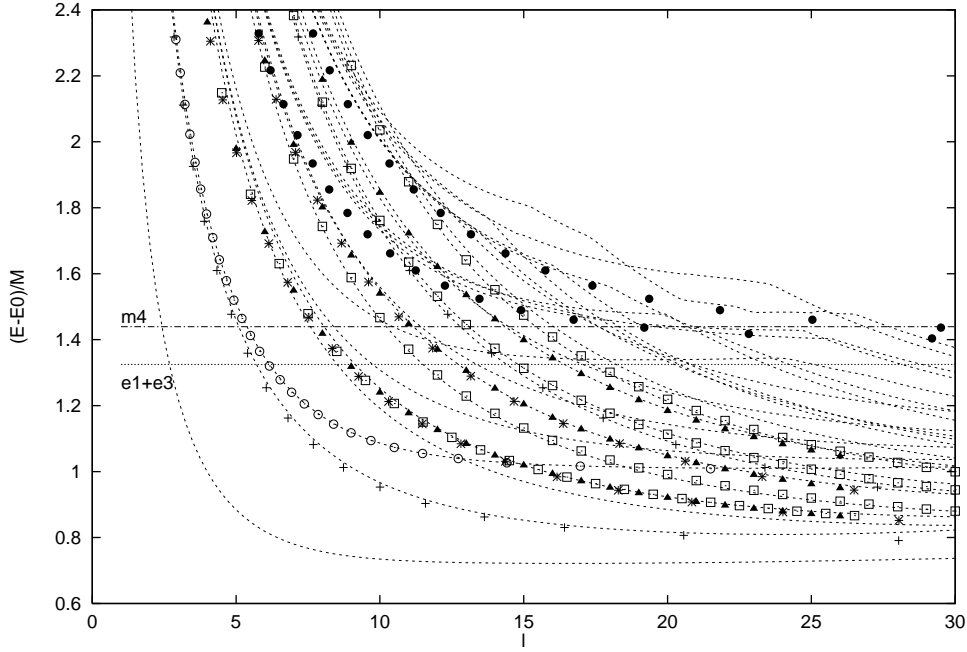


Figure 6.6: TCSA data, the state  $|1, 3\rangle$ , and “excited” BY lines in the  $\mathbf{C}$  even sector of the DN model with  $p = 50/391$ .

is in the vicinity of a pole corresponding to  $|k\rangle$  in the appropriate reflection factor). It is expected that in this way we describe more accurately the volume dependence of the energy of the state combined from the moving breather and  $|k\rangle$ .

Since the TCSA data are usually the better the lower the level is, we may hope to confirm the new reflection factors mainly for light particles reflecting on lowly excited boundaries. In the  $p$  range we investigated the first breather is the lightest particle, therefore on Fig.(6.6) we compare  $B^1$ 's BY line on the first excited boundary  $|1\rangle$ , and the TCSA data. The points marked by  $*$  correspond to  $I_1 = 1, 2$  in (6.11). The data, corresponding to the alternative description, using two particle  $B^1 B^1$  lines with one imaginary rapidity and one real one with quantum numbers  $I_1 = 1 \dots 3$  are marked by the full triangles; they give a somewhat better description of the TCSA lines. The four lines marked by the empty boxes correspond to two particle  $B^1 B^1$  lines with real rapidity and quantum numbers  $(1, 0)$ ,  $(-1, 1)$ ,  $(1, 2)$  and  $(-2, 2)$  respectively. The lines marked by  $\circ$  and  $+$  are soliton with  $N = 1$  and  $B^2$  on ground state boundary with  $I_{1/2} = \frac{1}{2}$ , and  $I_{1/2} = \frac{7}{2}$ , respectively; their function is to help the reader to identify the already known breather/soliton ground state BY lines. Finally, for comparison, we also included in this plot two lines - marked by  $\bullet$ -s; they are solitonic “excited” BY lines with  $N = 1, 2$ .

Summarizing, we can say, that for the first breather, the satisfactory agreement we find between the TCSA data and the various ways of describing its scattering on the first excited boundary gives support for the correctness of the new reflection factors. We expect that the relatively poor agreement between the (considerably higher) TCSA data and the “excited” solitonic BY lines could be improved by replacing the latter by two particle soliton- $B^1$  lines where the breather is moving with an imaginary rapidity. On Fig.(6.6) we also show examples of real two particle BY lines correctly describing TCSA data as well as instances, when a TCSA line is described by several BY lines. In the  $\mathbf{C}$  odd sector the lowest lying “excited” BY lines describe the scattering of  $B^2$  on  $|1\rangle$ ; we repeated also in this case the analysis described above

and obtained the same qualitative conclusions.

## 7 Conclusions

In this paper we analyzed the sine-Gordon model with Neumann boundary condition (SGN). In particular we established the spectrum of boundary states, developed a framework to describe finite size effects in boundary theories and used this framework together with TCSA to confirm the boundary states and the reflection factors.

Of the boundary states we showed that they can be labelled by an increasing sequence of positive integers  $n_i$  satisfying  $n_i < [\frac{\lambda}{2}]$ , and denoted as  $|n_1, \dots, n_k\rangle$ . For the states  $|n\rangle$  we showed that their energies coincide with that of the WKB quantized classical boundary breather. We realized the existence of the states  $|n, k\rangle$  by studying on the one hand the poles of the breather's reflection factors on non excited boundaries, and on the other, the poles of the soliton reflection factor  $P_{|n\rangle}(u)$  on the excited state  $|n\rangle$ . The novel feature of this study was that we computed also the residues of the Coleman-Thun diagrams and the reflection factors. This way we discovered that Coleman-Thun diagrams and creation of boundary bound states may coexist: this happens if the residue of the diagram is not sufficient to explain the residue of the reflection factor. Finally we proved that the new boundary states labelled by more than one integers can be generated successively by appropriate soliton reflections. We also determined all solitonic and breather reflection factors on these new states and explained their poles.

It is interesting to compare the labeling of boundary states here in SGN to that of in sine-Gordon model with Dirichlet boundary conditions [4]. In the latter case the labeling is more complicated: it consists of two sequences of positive integers. The explanation is that in the Dirichlet case, in contrast to the Neumann one, the solitons and the anti solitons generate different boundary states.

Moving from the infinite half line to a finite line segment, we gave the general form of Bethe-Yang equations for particles in finite volume with boundaries and used them to discuss the appearance of boundary bound states in this finite size setting. We showed in particular, that these states can be described as solutions of the BY equations with purely imaginary rapidity.

Finally we studied the finite volume spectrum of SGN by the truncated conformal space approach. We established, that the ground state energy density of this model coincides with that of the bulk SG and could also relate the ground state Neumann boundary energy to that of the Dirichlet one with  $\phi_0 = 0$ . The perfect agreement we found between certain lines in the TCSA spectrum and the one particle soliton/breather Bethe-Yang lines gives evidence that the reflection factors entering into the BY lines are indeed correct. We showed that the boundary bound states indeed appear in the TCSA spectra as predicted by the Bethe-Yang equations with purely imaginary rapidity. Finally in the TCSA data we found evidence for the existence of the new multi labelled states and also for the excited state reflections.

### Acknowledgements

We thank F. Wágner for his assistance in the early stages of the numerical work. G. T. thanks the Hungarian Ministry of Education for a Magyary Postdoctoral Fellowship. This research was supported in part by the Hungarian Ministry of Education under FKFP 0178/1999, 0043/2001 and by the Hungarian National Science Fund (OTKA) T029802/99.

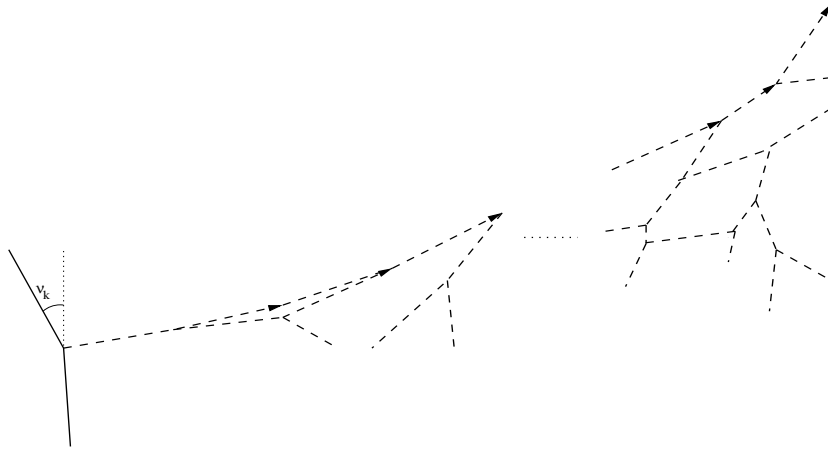


Figure A.1: Schematic draw of the top line

## A The proof of the existence of boundary bound states

In this appendix we prove that the boundary bound state  $|n_1, n_2, \dots, n_l, k\rangle$  can be created by reflecting a soliton with rapidity  $\nu_k$  on the boundary state  $|n_1, n_2, \dots, n_l\rangle$ . In doing so we show that no on-shell diagram exist for this process. Since any on-shell diagram consists of virtual processes we omit the attribute virtual from now on. One possible diagram is shown on Fig.(A.1).

The leftmost process in which a soliton arrives with rapidity  $\nu_k$  and virtually fuses with a breather into a soliton is called the final process while the breather is the final breather. Now if we follow the breather line towards the wall and turn in each 3-point vertex to the left we obtain a line which we call the top line. (In case of a 4-point vertex, that describes a possible two particle scattering instead of fusion, we follow the line with the same rapidity). The top line reaches the wall in the initial breather<sup>8</sup>. Of course we have analogous diagrams by replacing some of the breather lines with soliton lines. In this case the final/initial soliton terminology is used. Clearly in the final process the particle created must travel towards the wall i.e. it must have positive rapidity.

The outline of the proof goes as follows: First of all we introduce the notion of “proper” particles and show that particles with rapidity suitable for being final ones are “proper”. Since any initial particles are also “proper” we show that in the diagram above only “proper” particles exist. Moreover, we determine all the bulk processes that take place on the top line and call them “proper” processes. Having introduced a charge like quantity for “proper” particles we show that the maximal charge of the initial particles is  $n_l$ . Since the charge never increases in “proper” processes and the charge of the final particle is at least  $k$  which is larger than  $n_l$  we conclude that no on-shell diagram exists.

Let us go into the details. We call a breather “proper” if it has rapidity  $-u_n$ ,  $n \in N$  and a soliton is “proper” if its rapidity is  $-\nu_n$ . The possible final processes are shown by diagram (a-b) on Fig.(A.2). Clearly both the final breather and the final solitons are “proper”. Initial particles are produced by the decay of boundary bound states, the various virtual processes are described on the three diagrams of Fig.(A.3). Clearly all the initial particles are also “proper”.

---

<sup>8</sup>We call it in this way, because in our convention, when time flows from top to bottom, the emission of this breather by the wall precedes all the other processes on the top line.

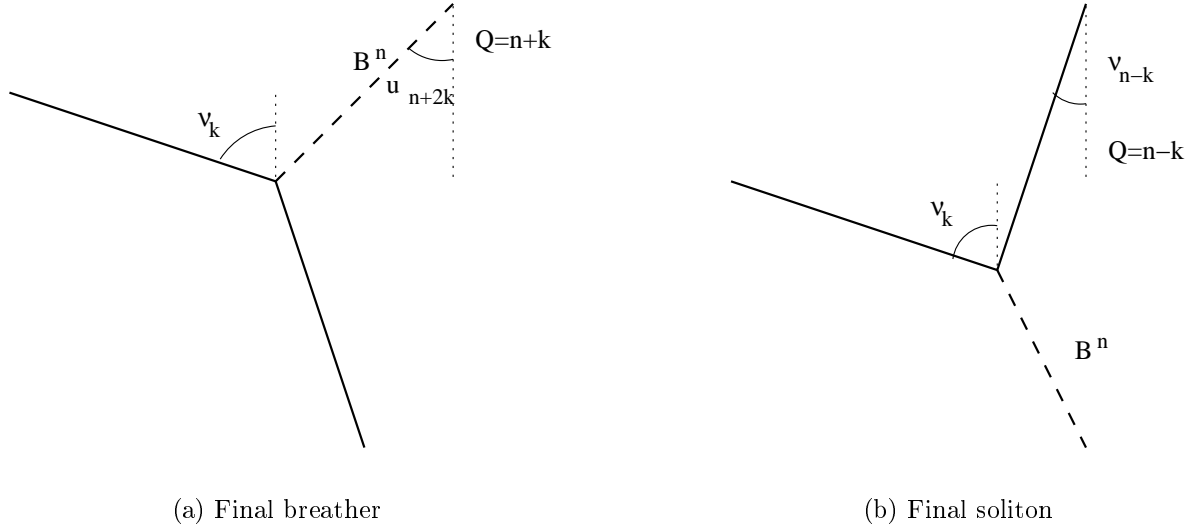


Figure A.2: Final processes

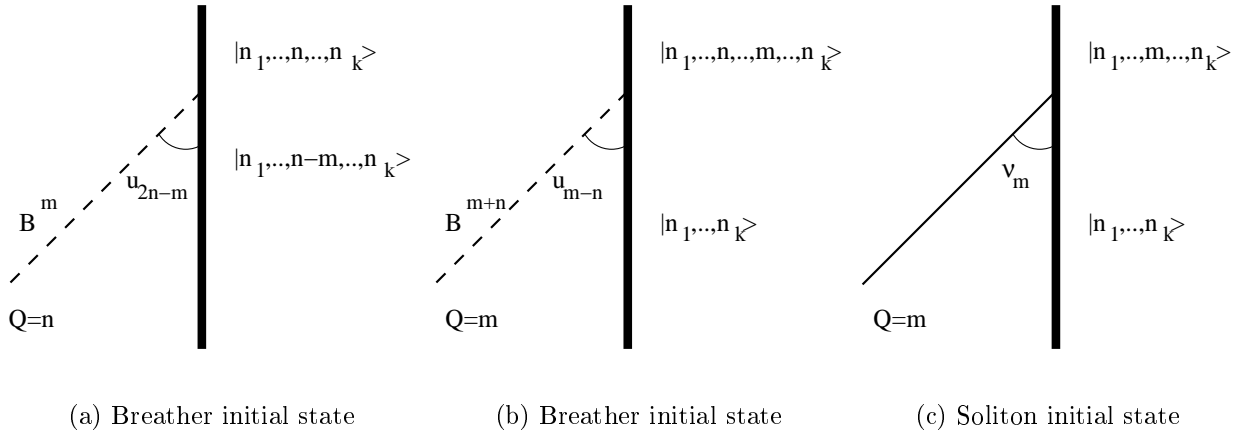


Figure A.3: Initial processes

For “proper” particles we introduce the notion of charge. For  $B^n$  with rapidity  $u = -u_m$  the charged is defined to be  $Q = \frac{n+m}{2}$  while for a soliton with rapidity  $u = -\nu_k$  it is simply  $Q = k$ . The charges of the initial particles are also displayed on Fig.(A.3). The maximum of the initial charge is  $n_l$ , obviously. The final charges are also displayed on Fig.(A.2). Since the particle, produced in the final process, has to travel towards the wall, (i.e.  $\nu_{n-k} < \nu_k$  for diagram (b)), we conclude that the final charge must be larger than  $k$ . Now we analyze how the charges change on the top line.

We are looking for bulk processes which can take place on the top line i.e. which are in between the final and initial “proper” particles. There are two types of bulk processes, one with only breathers and the other one with two solitons and one breather, already depicted on Fig.(3.1). In the present case however, any of the particles can arrive from the boundary so we have six different cases. First we analyze how the rapidities are changing. Consider the diagrams on Fig.(A.4-A.5).

We start with the case when the final particle is a breather. Let us denote, for a moment, by  $N_x$  the number of  $x$  type process on the top line, where  $x$  runs through the six diagrams

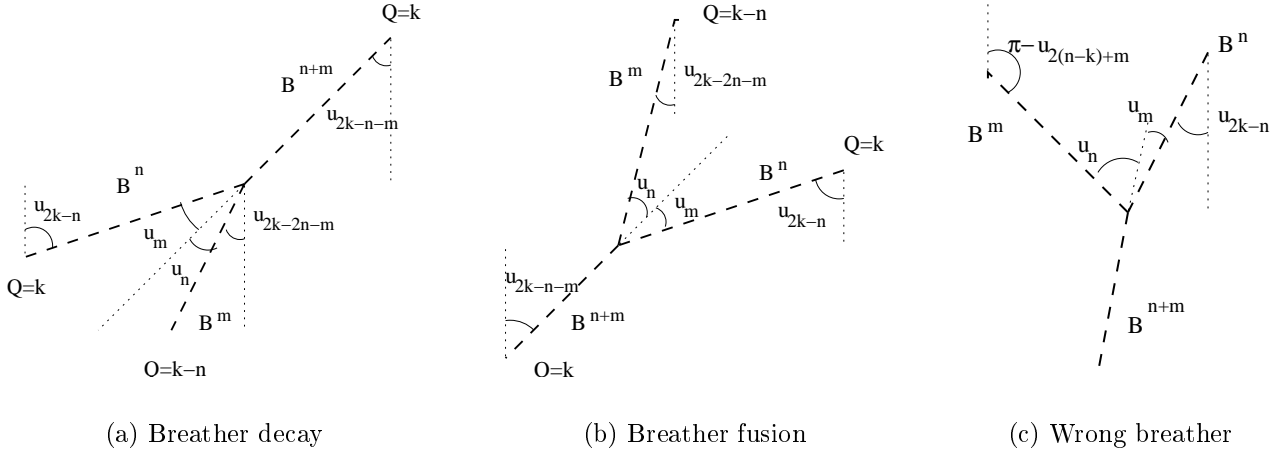


Figure A.4

on Fig.(A.4) and Fig.(A.5). From the conservation of particle types it follows that in case of a breather initial state  $N_{\text{breather-soliton}} = N_{\text{soliton-breather}}$ , while in case of a solitonic initial state  $N_{\text{breather-soliton}} + 1 = N_{\text{soliton-breather}}$  and all other  $N_x$ -s are unconstrained. We claim, however, that only diagrams (a-b) on Fig.(A.4) are allowed. In showing this we parameterize the rapidities as  $K\frac{\pi}{2} + u_n$  and note that for a “proper” breather  $K = 0$ , while for a “proper” soliton  $K = -1$ . Now it is easy to see that on diagrams (a-b) on Fig.(A.4) and on diagram (c) on Fig.(A.5) the parameter  $K$  does not change, on diagram (c) on Fig.(A.4)  $K \rightarrow K + 2$ , on diagram (a) on Fig.(A.5)  $K \rightarrow K - 1$ , finally on diagram (b) on Fig.(A.5)  $K \rightarrow K + 3$ . Since the initial and final particles are “proper” the various  $K$ -factors must sum up accordingly on the top line, showing that only diagrams (a-b) on Fig.(A.4) are allowed. We call these processes “proper”.

We also indicated on the diagrams how the charge changes. If we did not have diagram (b) on Fig.(A.4) we would be ready, since in the process on diagram (a) the charge never increases, consequently the final charge can not be larger than the initial one. In the general case, having also the breather fusion type process we argue as follows: find the breather fusion vertex on the top line which is farthest away from the wall. The bottom breather coming from the direction of the wall in this process is also a “proper” breather. Following its line back towards the wall always turning to the left we either reach the top line or the wall. Thus this new line has one or two common vertices with the top line. Now we change from the original top line to a new “top” line by replacing the segment of the the old one between the common vertices or between the common vertex and the wall with the line obtained from the bottom breather. Since the new line segment shares the properties of the original top line, namely it starts and ends with a “proper” breather and we have turned at each vertex to the left, we can argue for it in the same way as before. Applying this procedure step by step we arrive at a line which contains only breather decay type processes so the previous argument applies. Since in every step we eliminate at least one edge of the diagram the procedure terminates and we arrive at the final breather concluding that its charge can not be larger than the largest initial charge i.e.  $n_l$ .

For the solitonic final state the  $K$  parameter is  $-1$ . Thus either we have purely solitonic processes on the top line, in which case the charge decreases with each step or we start with some breather processes allowed in the above mentioned sense and later by the breather-soliton diagram on Fig.(A.5) we change back from the breather to soliton and continue with

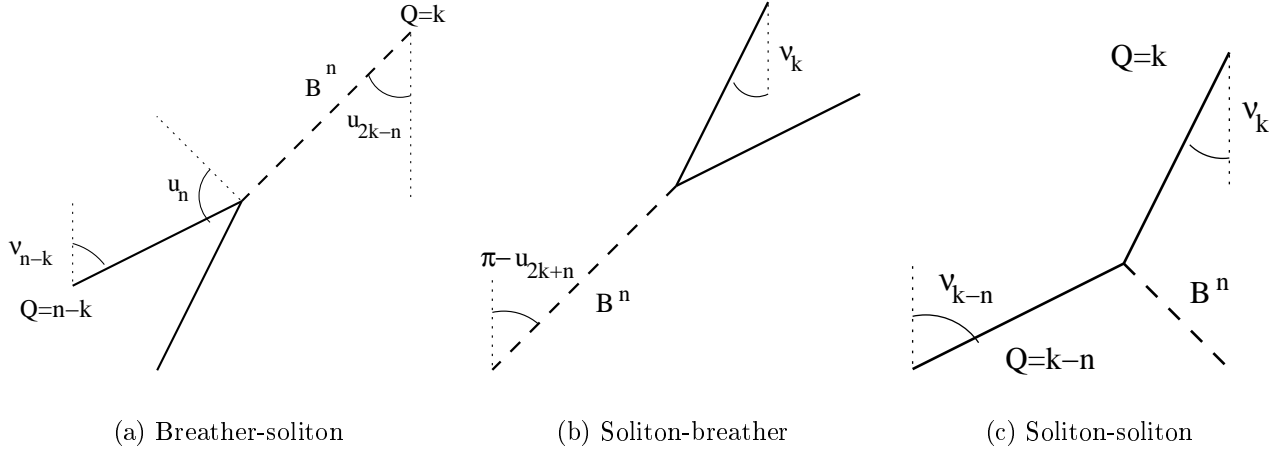


Figure A.5

the purely solitonic processes. Now in the second case the previous proof for the breathers can be used to show that the charge does not increase in the breather part of the top line. In the change from a breather to soliton the charge always decreases, since for  $B^n$  with charge  $k$  the inequality  $n < 2k$  is always satisfied, so the conclusion is the same i.e. the final charge is always less than the maximal initial charge  $n_l$ .

Summarizing we showed that no on-shell diagram exists, since for the existence the final charge must be at least  $k$ , but the initial charge is at most  $n_l < k$  and the charge does not increase in the allowed processes.

These considerations apply to the direct channel process only. The proof for the crossed channel is quite similar so we omit it here. The difference is just that we have to introduce a new charge for  $B^n$  which is  $q = \frac{n-m}{2}$  if the rapidity is  $u = u_m$ . Having analyzed the analogous diagrams step by step the conclusion is the same.

## B Pole structure

In this Appendix we start by reviewing the soliton and breather reflection factors on the state  $|n_1, n_2, \dots, n_k\rangle$  and analyze their pole structure. Proceeding inductively in the order of the pole we show nested on shell diagrams which have poles of the same order as the reflection amplitudes. We do not compute the residue of these diagrams, however, since on the one hand the calculation is very difficult to perform, and on the other, we know instances where the result does not coincide with the one coming from the reflection factor. The analysis is carried out in two steps. First, the solitonic poles are explained, then we turn to the explanation of the breather ones.

### B.1 Solitonic pole structure

The solitonic reflection factors are

$$P_{|n_1, n_2, \dots, n_k\rangle}(u) = a_{n_1}(u) a_{n_2}(u) \dots a_{n_k}(u) P(u) \quad ; \quad P \leftrightarrow Q \quad .$$

The function  $a_n(u) = \{2n - 1 + \lambda\} \{2n - 3 + \lambda\} \dots \{1 + \lambda\}$  has the pole structure shown on Fig.(B.1), where the number of dots represents the order of the pole.



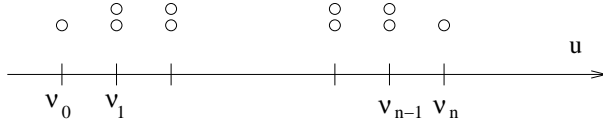


Figure B.1: Poles of  $a_n(u)$

In the general reflection amplitude we have to sum up all the orders of the poles of the various  $a_{n_i}(u)$  factors and also to take into account the poles of the prefactor  $P(u)$ . As a result, we have the following table

location	$\nu_1$	$\dots$	$\nu_{n_1-1}$	$\nu_{n_1}$	$\nu_{n_1+1}$	$\dots$	$\nu_{n_k-1}$	$\nu_{n_k}$	$\nu_{n_k+1}$	$\dots$	$\nu_{n_{max}}$
order	$2k+1$	$\dots$	$2k+1$	$2k$	$2k-1$	$\dots$	3	2	1	$\dots$	1

Now the main observation, similar to what was made in [4], is that the poles above are already present in the reflection amplitude  $P_{[n_k]}(u)$ , only the orders are different, but this can be compensated by nesting appropriate sub-diagrams as we will see. Let us consider the poles at  $\nu_N$  step by step.

- As we proved in the previous Appendix the simple pole for  $N > n_k$  is responsible for the creation of the state  $|n_1, n_2, \dots, n_k, N\rangle$ .
- Lets consider diagram (a) on Fig.(B.3). The state  $|n_1, n_2, \dots, n_{k-1}, n_k\rangle$  decays to  $|n_1, n_2, \dots, n_{k-1}\rangle$  by emitting an anti soliton with rapidity  $\nu_{n_k}$ . The soliton and the anti soliton fuse into  $B^{N+n_k}$  with rapidity  $u_{n_k-N}$ . In the  $N = n_k$  case the breather travels parallel with the wall giving a diagram with a second order pole.
- In the  $N < n_k$  case the reflection factor of  $B^{N+n_k}$  has a pole at  $u = u_{n_k-N}$ , for which a sub-diagram, that is described in detail in the next subsection, has to be embedded. We just present here in advance, that when  $N$  decreasingly reaches any of the  $n_i$ -s then the order of the breather pole is increased by one and when  $N = n_i - 1$  it increases by one more. Furthermore, it does not change until  $N$  reaches  $n_{i-1}$ , where the same story happens. Collecting all the order of these poles and also the one more extra, which comes from the ground state reflection factor we arrive at the right result.

We emphasize that from the shifting argument described in section (3.3) we know that in spite of the existence of the on-shell diagram shown above the pole at  $\nu_N$  in the reflection amplitude  $P_{[n_1, n_2, \dots, n_k]}(u)$  also creates the state  $|n_1, \dots, n_i, N, n_{i+1}, \dots, n_k\rangle$ , if this state exists, that is if  $n_i < N < n_{i+1}$  for some  $i$ .

## B.2 Breather pole structure

The breather  $B^n$  on the state  $|n_1, n_2, \dots, n_k\rangle$  has the following reflection factor

$$R_{|n_1, n_2, \dots, n_k\rangle}^{(n)}(u) = b_{n_1}^n(u) b_{n_2}^n(u) \dots b_{n_k}^n(u) R^{(n)}(u)$$

where

$$b_m^n(u) = \{n+2m-1\} \{n+2m-3\} \dots \{n+2m-1-2l\} \dots \begin{cases} \{n-2m+1\} & \text{if } n-2m+1 > 0 \\ \{2m-n+1\} & \text{if } 2m-n+1 > 0 \end{cases} .$$

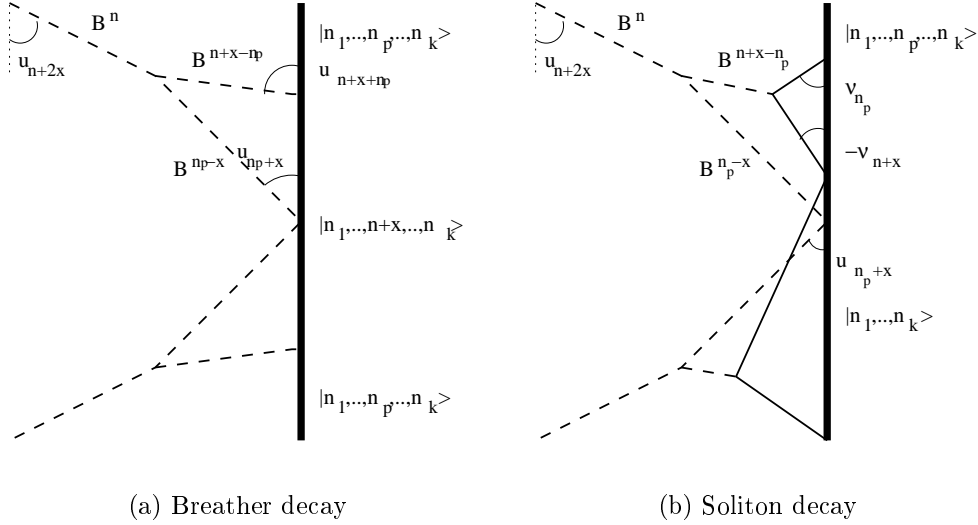
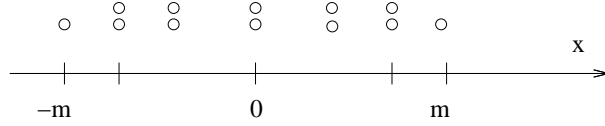
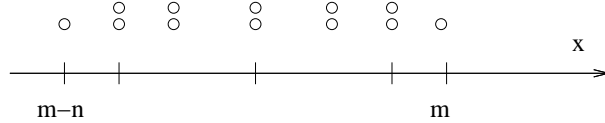


Figure B.2

Lets parameterize the poles of  $b_m^n(u)$  as  $u_{n+2x}$ . Considering the two cases separately we obtain the location of the poles as



in the case when  $n > 2m$  while as



in the other case. Summing up all the poles coming from the various  $b$ -factors we get the following result. If  $n_q \leq x < n_{q+1}$  and  $n_p \leq n+x < n_{p+1}$  hold in the  $x > 0$  case or  $n_q \leq |x| < n_{q+1}$  and  $n_p < n-|x| < n_{p+1}$  is satisfied for  $x < 0$ , then the order of the pole at  $u_{n+2x}$  is  $2(p-q) + \epsilon$  (where  $\epsilon = 1$  if the bound for  $p$  is saturated and  $\epsilon = -1$  if the bound for  $q$  is saturated and zero otherwise). For each pole there is the analogous pole at  $\pi - u_{n+2x}$ , which is in the physical strip if  $u_{n+2x}$  is not there.

Now we explain the pole of the reflection amplitude  $R_{|n_1, n_2, \dots, n_k\rangle}^{(n)}(u)$  at  $u_{n+2x}$ . For  $x = n_k$  the state  $|n_1, n_2, \dots, n_k + n\rangle$  is created or if it is not in the spectrum we have an analogous diagram to diagram (d) on Fig.(3.2). For  $x < n_k$  consider diagram (a) on Fig.(B.2).

Here  $B^n$  decays into  $B^{n+x-n_p}$  and  $B^{n_p-x}$  in the bulk. First  $B^{n+x-n_p}$  reaches the wall with rapidity  $u_{n+x+n_p}$  exciting the state  $|n_1, \dots, n_p, \dots, n_k\rangle$  to  $|n_1, \dots, n+x, \dots, n_k\rangle$ . If the breather traveled backwards in time ( $n+x+n_p > [\lambda]$ ) or the excited state did not exists ( $n+x > [\frac{\lambda}{2}]$ ) then we would have diagram (b), where the state  $|n_1, \dots, n_{p-1}, n_p, n_{p+1}, \dots, n_k\rangle$  would decay to  $|n_1, \dots, n_{p-1}, n_{p+1}, \dots, n_k\rangle$  by the emission of a soliton with rapidity  $-\nu_{n_p}$ , which then absorbs  $B^{n+x-n_p}$  and reaches the wall at rapidity  $-\nu_{n+x}$ . In both cases  $B^{n_p-x}$  reflects on the resulting state with rapidity  $u_{(n_p-x)+2x}$ . In order to compute the order of its pole we observe that  $n_q \leq x < n_{q+1}$  as before, but now  $n_{p-1} < (n_p-x)+x$ . From this it follows

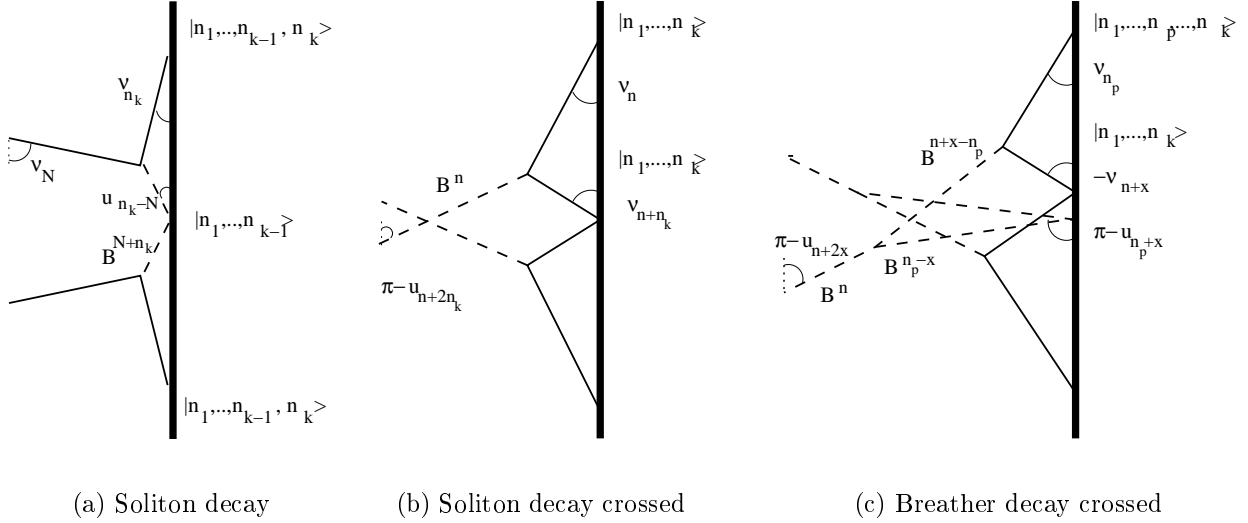


Figure B.3

that the order of the pole is  $2(p-1-q)+\epsilon$ , which is less than the one investigated originally by two. Since the diagram itself gives a second order pole (we have used the Coleman-Thun type cancellation in the (b) case) we are ready. Resolving inductively the pole of this reflection by the analogous sub-diagram we arrive at cascades of diagrams, where in the last sub-diagram the breather reflects with a simple pole or without poles.

For the poles of type  $\pi - u_{n+2x}$  we have an analogous consideration: If we parameterize the rapidity as  $\pi - u_{n+2x}$  and analyze the relation between  $x, n+x$  and  $n_i$  we get the same formula for the order of the poles as we had before. The explanation is given in terms of the crossed diagrams. Diagram (b) on Fig.(B.3) explains the  $x = n_k$  case, while for  $x < n_k$  we have diagram (c) on the same Figure. The argument is completely analogous to the non-crossed version so we omit it here.

Note, that these breather diagrams are generic, which means that they exist for any  $x$ . It may happen, however, that for some particular  $x$  we have some other diagram with the right order of pole. Notice also that in spite of the existence of the diagrams above we might have boundary bound state creation, described in detail in section (3.3), at the same time.

## C Boundary $c = 1$ theories

In this Appendix we warm up by considering the compactified free boson with periodic boundary conditions on a circle of circumference  $L$ . Having mapped the system onto the plane we identify those conformally invariant boundary conditions which also preserve the underlying affine  $\hat{U}_1 \times \hat{U}_1$  symmetry. They originate from cutting the original circle and applying Neumann or Dirichlet boundary conditions on both ends of the strip. We also determine the theory which corresponds to imposing Neumann boundary condition on one end and Dirichlet boundary condition on the other end of the strip. In all cases the data we need for the TCSA, such as the spectrum of bulk and boundary primary operators, their normalizations, conformal weights, bulk and boundary operator product expansions are summarized. Though most of these data are available in the literature we collect them here to make the paper self

contained.

## C.1 Compactified free boson with periodic boundary conditions

Consider a free boson with compactification radius  $r$  confined into a box of size  $L$  subject to periodic boundary condition  $\Phi(L, t) \equiv \Phi(0, t) + 2\pi r n$ , where  $n \in \mathbb{Z}$  is called the winding number. The action which governs the dynamics is

$$S = \frac{1}{8\pi} \int_{-\infty}^{\infty} dt \int_0^L dx \partial_\mu \Phi \partial^\mu \Phi$$

Canonical quantization results in the following expression for the field operator  $\Phi(x, t)$ :

$$\Phi(x, t) = \Phi_0 + \frac{4\pi}{L} \left( \Pi_0 t + \frac{rM}{2} x \right) + i \sum_{n \neq 0} \frac{1}{n} \left( a_n e^{i \frac{2\pi}{L} n(x-t)} + \bar{a}_n e^{-i \frac{2\pi}{L} n(x+t)} \right),$$

where  $M$  is the winding operator with eigenvalues  $m \in \mathbb{Z}$ , and the nonzero commutators are

$$[\Phi_0, \Pi_0] = i \quad ; \quad [a_n, a_m] = n \delta_{n+m} \quad , \quad [\bar{a}_n, \bar{a}_m] = n \delta_{n+m} \quad . \quad (\text{C.1})$$

We can use  $\zeta$ -function regularization for computing the Casimir energy and find the Hamiltonian as

$$H = \frac{2\pi}{L} \sum_{n>0} (a_{-n} a_n + \bar{a}_{-n} \bar{a}_n - \frac{1}{12}) + \frac{2\pi}{L} \left( \Pi_0^2 + \left( \frac{rM}{2} \right)^2 \right) .$$

Having mapped the system onto the plane via the  $(x, it) = \xi \rightarrow z = e^{i \frac{2\pi}{L} \xi}$  conformal transformation, chiral factorization originates from the split  $\Phi(z, \bar{z}) = \phi(z) + \bar{\phi}(\bar{z})$ , where

$$\phi(z) = \phi_0 - i a_0 \ln z + i \sum_{n \in \mathbb{Z}} a_n \frac{z^{-n}}{n} \quad ; \quad \bar{\phi}(\bar{z}) = \bar{\phi}_0 - i \bar{a}_0 \ln \bar{z} + i \sum_{n \in \mathbb{Z}} \bar{a}_n \frac{\bar{z}^{-n}}{n} .$$

It is useful to introduce the dual of  $\Phi(z, \bar{z})$  as  $\tilde{\Phi}(z, \bar{z}) = \phi(z) - \bar{\phi}(\bar{z})$ . The  $\hat{U}_1 \times \hat{U}_1$  symmetry of the model is generated by the chiral currents,  $J(z) = i \partial_z \phi(z)$ ,  $\bar{J}(\bar{z}) = i \partial_{\bar{z}} \bar{\phi}(\bar{z})$ , and the primary fields of the symmetry algebra are the vertex operators

$$V_{(n,m)}(z, \bar{z}) = : e^{i \frac{n}{r} \Phi(z, \bar{z}) + i \frac{m r}{2} \tilde{\Phi}(z, \bar{z})} := : e^{i q \phi(z) + i \bar{q} \bar{\phi}(\bar{z})} : \quad (\text{C.2})$$

We use the parameterization  $(n, m)$  and  $(q, \bar{q})$  in parallel, the connection between them being  $q + \bar{q} = \frac{2n}{r}$  and  $q - \bar{q} = m r$ . The vertex operators have conformal weights  $h_{(n,m)} = \frac{q^2}{2}$ ,  $\bar{h}_{(n,m)} = \frac{\bar{q}^2}{2}$  with respect to the conformal energy momentum tensor  $T(z) = \frac{1}{2} : J(z) J(z) :$  and  $\bar{T}(\bar{z}) = \frac{1}{2} : \bar{J}(\bar{z}) \bar{J}(\bar{z}) :$ . The Hilbert space is built up by the successive application of the modes of the chiral currents on the highest weight state created by the vertex operators as

$$|n, m\rangle = V_{(n,m)}(0, 0)|0\rangle$$

and  $\Pi_0 |n, m\rangle = n |n, m\rangle$ ,  $M |n, m\rangle = m |n, m\rangle$ . The operator product expansion of the vertex operators starts as

$$V_{(q,\bar{q})}(z, \bar{z}) V_{(q',\bar{q}')}(\bar{w}, w) = (z - w)^{q q'} (\bar{z} - \bar{w})^{\bar{q} \bar{q}'} V_{(q+q', \bar{q}+\bar{q}')}(\bar{w}, w) + \dots \quad (\text{C.3})$$

We have two maximal sets of the allowed  $(n, m)$  pairs [19] and here we concentrate on the bosonic one which has  $n \in \mathbb{Z}, m \in \mathbb{Z}$ .

## C.2 Conformal boundary conditions

Now we would like to impose such boundary conditions in the theory that preserve not only the conformal but also the Kac-Moody symmetry of the model. The easiest way to formulate this is to restrict the theory on the upper half plane and demand[20]

$$L(z) = \bar{L}(\bar{z}) \quad , \quad J(z) = \Omega \bar{J}(\bar{z}) \quad ;$$

on the real axis, where  $\Omega$  is any automorphism of the algebra (C.1). We have two possible choices  $\Omega = 1$  or  $\Omega = -1$ , [21], they correspond to Neumann and Dirichlet boundary conditions imposed on the field  $\Phi$ , respectively. Note that for the dual field the roles are interchanged, that is  $\Omega = 1$  corresponds to Dirichlet while  $\Omega = -1$  for Neumann boundary condition.

### C.2.1 Neumann boundary condition

The  $\Omega = 1$  boundary condition in terms of the modes reads as  $\bar{a}_n = a_n$ , that is

$$\Phi(z, \bar{z}) = \Phi_0 - ia_0(\ln z + \ln \bar{z}) + i \sum_{n \in \mathbb{Z}} \frac{a_n}{n} (z^{-n} + \bar{z}^{-n}) .$$

We can map this field back to the strip by the inverse of the transformation  $\xi \rightarrow z = e^{i\frac{\pi}{L}\xi}$

$$\Phi(x, t) = \Phi_0 + \frac{4\pi}{L}\Pi_0 + \sum_{n \neq 0} \frac{a_n}{n} (e^{i\frac{\pi}{L}n(x-t)} + e^{-i\frac{\pi}{L}n(x+t)}) \quad (C.4)$$

From the  $x$ -dependence we can read off the Neumann boundary conditions

$$\partial_x \Phi(0, t) = \partial_x \Phi(L, t) = 0 \quad ; \quad \forall t$$

The Hamiltonian of this system in the strip can be obtained directly from (C.4) by  $\zeta$ -function regularization

$$H = \frac{2\pi}{L}\Pi_0^2 + \frac{\pi}{L} \left( \sum_{n \neq 0} n a_{-n} a_n - \frac{1}{24} \right) . \quad (C.5)$$

Turning back to the plane we realize that the vertex operators  $V_{(n,0)}(z, \bar{z})$  do not reproduce the most singular part of the OPE (C.3) any more as we would expect. Changing however their normalization function as

$$V_{(n,0)}(z, \bar{z}) = |z - \bar{z}|^{q^2} : e^{iq\Phi(z, \bar{z})} : \quad ; \quad q = \frac{n}{r} , \quad (C.6)$$

we preserve their conformal weights, (which is  $h = \frac{q^2}{2}$  for  $T(z)$ ) and restore the leading part of the OPE (C.3). The boundary fields in a boundary conformal field theory live only on the boundary and are in a one-to-one correspondence with the vectors of the Hilbert space. In our case they are the boundary vertex operators

$$\Psi_q(x) = : e^{iq\Phi(x,x)} : \quad ; \quad q = \frac{n}{r} ,$$

(which are primary fields of weight  $h_n = 2q^2$ ), and their descendants. The dual field vanishes at the boundary so in the Hilbert space we do not have winding as we would expect from the Neumann boundary condition.

### C.2.2 Dirichlet boundary condition

The  $\Omega = -1$  boundary condition forces  $\Phi(z, \bar{z})$  to be of the form

$$\Phi(z, \bar{z}) = \Phi_0 - ia_0(\ln z - \ln \bar{z}) + i \sum_{n \in \mathbb{Z}} \frac{a_n}{n} (z^{-n} - \bar{z}^{-n}) .$$

The boundary condition can be determined on the strip by mapping the system via the inverse of  $\xi \rightarrow z = e^{i\frac{\pi}{L}\xi}$  to the strip. We have

$$\Phi(x, t) = \Phi_0 + \frac{2\pi}{L} r \tilde{M} x - i \sum_{n \neq 0} \frac{a_n}{n} \left( e^{i\frac{\pi}{L}n(x-t)} - e^{-i\frac{\pi}{L}n(x+t)} \right) ,$$

where  $\tilde{M} = M + \frac{\Phi_L - \Phi_0}{2\pi r}$  and  $M \in \mathbb{Z}$  is the winding number. This corresponds to the

$$\Phi(0, t) = \Phi_0 \quad ; \quad \Phi(L, t) = \Phi_L \quad \forall t$$

Dirichlet boundary condition. The Hamiltonian of the system above is

$$H = \frac{2\pi}{L} \left( \frac{r\tilde{M}}{2} \right)^2 + \frac{\pi}{L} \left( \sum_{n \neq 0} n a_{-n} a_n - \frac{1}{24} \right) . \quad (\text{C.7})$$

By changing the normalization function of the vertex operators

$$V_{(q,0)}(z, \bar{z}) = |z - \bar{z}|^{-q^2} : e^{iq\Phi(z, \bar{z})} : \quad ; \quad q = \frac{n}{r} , \quad (\text{C.8})$$

we can ensure the most singular part of the bulk OPE to hold. Now the field  $\Phi$  is constant at the boundary so we do not have nonzero momentum Fock modules. The dual field however can create the sectors corresponding to the different winding numbers. The Hilbert space by this token consists of the Fock modules corresponding to the different winding numbers.

### C.2.3 Mixed boundary condition

It is also possible to demand mixed boundary conditions. On the plane one possible choice is Dirichlet boundary condition for  $\Im m(z) = 0$ ,  $\Re e(z) > 0$  and Neumann for  $\Im m(z) = 0$ ,  $\Re e(z) < 0$ . A field satisfying this can be given as

$$\Phi(z, \bar{z}) = \Phi_0 + i \sum_{n \in \mathbb{Z} + \frac{1}{2}} \frac{a_n}{n} (z^{-n} - \bar{z}^{-n}) .$$

Since on the strip

$$\Phi(x, t) = \Phi_0 - i \sum_{n \in \mathbb{Z} + \frac{1}{2}} \frac{a_n}{n} \left( e^{i\frac{\pi}{L}n(x-t)} - e^{-i\frac{\pi}{L}n(x+t)} \right) ,$$

the boundary condition there reads as

$$\Phi(0, t) = \Phi_0 \quad ; \quad \partial_x \Phi(L, t) = 0 \quad \forall t ,$$

that is Dirichlet boundary condition at  $x = 0$  and Neumann boundary condition at  $x = L$ . Using  $\zeta$ -function regularization the Hamiltonian turns out to be

$$H = \frac{\pi}{L} \left( \sum_{n \in \mathbb{Z} + \frac{1}{2}} n a_{-n} a_n + \frac{1}{48} \right). \quad (\text{C.9})$$

The model looks like a twisted boson with chiral current  $J(z) = \sum_{n \in \mathbb{Z} + \frac{1}{2}} a_n z^{-n-1}$ . The vertex operators acquire a factor

$$V_q(z, \bar{z}) = \left( \frac{\sqrt{\frac{z}{\bar{z}}} + 2 + \sqrt{\frac{\bar{z}}{z}}}{4|z - \bar{z}|} \right)^{q^2} : e^{iq\Phi(z, \bar{z})} : \quad ; \quad q = \frac{n}{r}, \quad (\text{C.10})$$

in order to ensure the most singular part of the bulk OPE to hold. Now the field  $\Phi$  has a non vanishing limit only for  $\Im m(z) = 0$ ,  $\Re e(z) < 0$  while the dual field survives at  $\Im m(z) = 0$ ,  $\Re e(z) > 0$ . Thus the only boundary operator is the current  $J(x)$  and consequently the Hilbert space is generated by acting with its modes  $a_{-n}$ ,  $n \in \mathbb{Z}_+ - \frac{1}{2}$ , on the vacuum vector.

## References

- [1] S. Ghoshal and A. Zamolodchikov, *Int. J. Mod. Phys.* **A9** (1994) 3841 ([hep-th/9306002](#)).
- [2] H. Saleur. *Lectures on non perturbative field theory and quantum impurity problems* in the proceedings of the 1998 Les Houches Summer School [cond-mat/9812110](#)  
H. Saleur. *Lectures on non perturbative field theory and quantum impurity problems Part II* [cond-mat/0007309](#)
- [3] S. Ghoshal, *Int. J. Mod. Phys.* **A9** (1994) 4801 ([hep-th/9310188](#)).
- [4] P. Mattsson and P. Dorey, *J. Phys.* **A33** (2000) 9065. ([hep-th/0008071](#))
- [5] S. Skorik and H. Saleur *J. Phys.* **A28** (1995) 6605. ([hep-th/9502011](#))
- [6] S. Coleman and H.J. Thun *Comm. Math. Phys.* **61** (1978) 31.
- [7] P. Dorey, R. Tateo and G. Watts *Phys. Lett.* **B448** (1999) 249 ([hep-th/9810098](#)).
- [8] V.P. Yurov and Al.B. Zamolodchikov *Int. J. Mod. Phys.* **A6** (1991) 1125.
- [9] R.F. Dashen, B. Hasslacher and A. Neveu, *Phys. Rev.* **D11** (1975) 3424.
- [10] A.B. Zamolodchikov and Al.B. Zamolodchikov *Ann. Phys.* **120** (1979) 253.
- [11] Z. Bajnok, L. Palla, G. Takács and G. Zs. Tóth in preparation
- [12] P. Fendley and H. Saleur *Nucl. Phys.* **B428** (1994) 681. ([hep-th/9402045](#))
- [13] H.G. Kausch, G. Takacs and G. Watts *Nucl. Phys.* **B489** (1997) 557. ([hep-th/9605104](#))

- [14] P. Dorey, A. Pocklington, R. Tateo and G.M.T. Watts *Nucl. Phys.* **B525** (1998) 641.  
(hep-th/9712197)
- [15] K. Graham, I. Runkel and G.M.T. Watts *Renormalization flows of boundary theories*  
hep-th/0010082  
K. Graham, I. Runkel and G.M.T. Watts *Minimal boundary flows and  $c = 1$  CFT*  
hep-th/0101187
- [16] G. Feverati, F. Ravanini and G. Takács, *Nucl. Phys.* **B540** (1999) 543-586,  
(hep-th/9805117).  
G. Feverati, F. Ravanini and G. Takács, *Phys. Lett.* **B444** (1998) 442-450,  
(hep-th/9807160).
- [17] Al.B. Zamolodchikov, *Int. J. Mod. Phys.* **A10** (1995) 1125.
- [18] A. LeClair, G. Mussardo, H. Saleur, and S. Skorik *Nucl. Phys.* **B459** (1995) 581.  
(hep-th/9503227)
- [19] T.R. Klassen and E. Melzer, *Int. J. Mod. Phys.* **A8** (1993) 4131.
- [20] V. B. Petkova and J.-B. Zuber, *Conformal Boundary Conditions and what they teach us*,  
hep-th/0103007.
- [21] A. Recknagel, V. Schomerus, *Nucl.Phys.* **B545** (1999) 233-282.